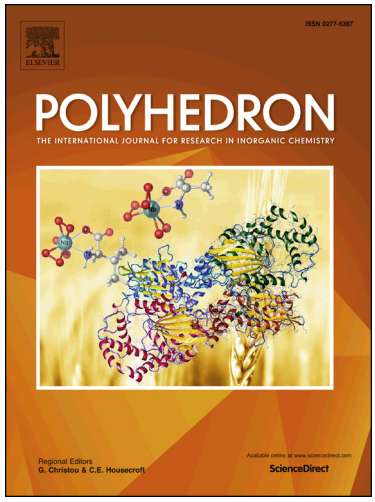

DNA Interaction and Anticancer Evaluation of New Palladium(II), Platinum(II) and Silver(I) Complexes Based on (Δ)- and (Λ)-1,2–Bis-(1H-benzimidazol-2-yl)-1,2-ethanediol Enantiomers

Ahmed A. Shabana, Ian S. Butler, Annie Castonguay, Mohsen Mostafa, Bertrand J. Jean-Claude, Sahar.I. Mostafa

PII: S0277-5387(18)30407-8
DOI: https://doi.org/10.1016/j.poly.2018.07.020
Reference: POLY 13285

To appear in: *Polyhedron*

Received Date: 10 March 2018
Revised Date: 2 July 2018
Accepted Date: 3 July 2018

Please cite this article as: A.A. Shabana, I.S. Butler, A. Castonguay, M. Mostafa, B.J. Jean-Claude, Sahar.I. Mostafa, DNA Interaction and Anticancer Evaluation of New Palladium(II), Platinum(II) and Silver(I) Complexes Based on (Δ)- and (Λ)-1,2–Bis-(1H-benzimidazol-2-yl)-1,2-ethanediol Enantiomers, *Polyhedron* (2018), doi: https://doi.org/10.1016/j.poly.2018.07.020

DNA Interaction and Anticancer Evaluation of New Palladium(II), Platinum(II) and Silver(I) Complexes Based on (Δ)- and (Λ)-1,2–Bis-(1H-benzimidazol-2-yl)-1,2-ethanediol Enantiomers

Ahmed A. Shabana[1], Ian S. Butler[2,*], Annie Castonguay[3], Mohsen Mostafa[1], Bertrand J. Jean-Claude[4], Sahar. I. Mostafa[1,*]

[1] Chemistry Department, Faculty of Science, Mansoura University, Mansoura 35516, Egypt

[2]Department of Chemistry, McGill University, Montreal QC, Canada H3A 2K6

[3] INRS-Institut Armand-Frappier, Institut National de la Recherche Scientifique, Université du Québec, Laval, Canada

[4]McGill University, Royal Victoria Hospital, Department of Medicine, Montreal, QC H3A 1A1, Canada

E-mail: ian.butler@mcgill.ca & sihmostafa@gmail.com

Tel: 002-01008502625

Fax: 0020502246781

Abstract

The synthesis of some new palladium(II), platinum(II) and silver(I) complexes based on (Δ)- and (Λ)-1,2–bis-(1H-benzimidazol-2-yl)-1,2-ethanediol (Δ-H_2bie and Λ-H_2bie) enantiomers in the absence and presence of the N,N-chelates 2,2'-bipyridyl and 9,10-phenanthroline, and triphenylphosphine is reported. The molecular structures of the new complexes are discussed on the basis of their IR, Raman, UV–Vis, NMR (^{1}H, ^{13}C and ^{31}P) and mass spectra, elemental analyses, molar conductivities and TGA properties. Both Δ-H_2bie and Λ-H_2bie coordinate to the metal ions in a neutral bidentate manner through the azomethine-N and protonated hydroxy-O

atoms, while in basic media, Δ-Hbie$^-$ and Λ-Hbie$^-$ are bound to the metal ions through the azomethine-N and deprotonated-O atoms as mono-negative bidentate chelating ligands. The *in vitro* anticancer activity of the complexes has been evaluated against the human breast cancer (MDA-MB231) and ovarian cancer (OVCAR-8) cell lines. The Δ-H_2bie complexes are more active against the studied cell lines. The IC_{50} values for cell growth proliferation of [Ag(PPh_3)(Λ-H_2bie)]ClO_4 and [Ag(PPh_3)(Δ-Hbie)] are 0.443 and 1.277 μM, and 0.427 and 1.437 μM for the MDAMB231 and OVCAR-8 cell lines, respectively. The corresponding IC_{50} values for *cisplatin* were 3.20 (MDA-MB231) and 2.28 (OVCAR-8) μM. The DNA-binding properties of some of the complexes have been studied using circular dichroism (CD) spectroscopy. The results indicate that the complexes may have intercalative CT-DNA binding capabilities. The intercalation of the Δ-enantiomers appears to be greater than is that for the Λ- enantiomers. Insertion of the complexes into adjacent base pairs prevents neighboring base pairs from close stacking.

Keywords: Δ-H_2bie and Λ-H_2bie, palladium, platinum, silver, spectra, anticancer, DNA.

1. Introduction

Benzimidazoles constitute a class of heterocyclic aromatic organic compounds that contain a benzene ring fused to an imidazole ring. The most prominent benzimidazole compound found in nature is *N*-ribosyldimethylbenzimidazole, which serves as an axial ligand for Co(III) ions in vitamin B_{12} [1]. Benzimidazole and its derivatives are involved in various biological processes [2-5]. Substituted benzimidazoles are of interest since substitution at the 1, 2 and 5 positions has been shown to be related to their pharmacological properties [6]. In addition, the benzimidazole

scaffold is considered to be a useful structural motif in the development of therapeutic agents that display a broad spectrum of pharmacological activity. To date, many DNA minor groove binders containing one or more imidazole heterocycles have been reported that have promising anticancer and antiparasitic activities [7].

The synthesis and *in vitro* anticancer activities of *bis*-benzimidazole Zn(II) [7,8], Co(II) [8] and Cu(II) [9,10] derivatives have been reported. In addition, monomeric and polymeric mixed-ligand benzimidazole and malonic acid Co(II) and Cu(II) complexes has been described [11]. The preparation of the complexes $[Cr(2gb)_3]Cl[ZnCl_4]\cdot CH_3OH$, $[Cr(2gb)_3]Cl_3\cdot 4H_2O$ and $[Cr_2(2gb)_4(\mu\text{-}OH)_2](ClO_4)_4\cdot 5H_2O$ (2gb = 2-guanidinobenzimidazole) has been published [12], and the X-ray crystal structure of the latter binuclear complex revealed the presence of two 2gb moieties and a symmetric $(\mu\text{-}OH)_2$ bridge.

Tridentate facial chiral ligands deserve attention as they offer different types of binding sites with a view to enantioselective catalysis, so the introduction of chirality in the ligands is an attractive prospect. The synthesis and coordination chemistry of 1,2-bis(1*H*-benzimidazol-2-yl)-1,2-ethanediol and its methylated derivative indicate that they are versatile chiral, tridentate facially coordinating ligands (Scheme 1) [13]. The related 1,2-bis(2-benzimidazolyl) ethanol ligand, which is formed using malic acid instead of tartaric acid, can act as a facially coordinating tridentate ligand, with the -OH group coordinating to a Ni(II) ion in an octahedral geometry [14]. 1,2-Bis(1*H*-benzimidazol-2-yl)-1,2-ethanediol and its methylated derivative act as chiral, facially coordinating tridentate ligands, forming $[Cu(SS\text{-}1)_2](ClO_4)_2$ and $[Cu(SS\text{-}2)_2](ClO_4)_2$ [14]. The fully protonated structures were determined for the $[Ni(RR\text{-}\mathbf{1})_2]^{2-}$ and $[Ni(SS\text{-}\mathbf{1})_2]^{2-}$ complexes, which were formed from a racemate of the ligand and show homochirality [14]. On the other hand, the mono-deprotonated complex with a dimeric structure, $[Ni(RR\text{-}\mathbf{2})_2Ni(RR\text{-}\mathbf{2}\text{-}H)_2]^{2-}$, shows the

coordinated -OH groups of one complex molecule are hydrogen bonded to the coordinated alkoxide groups of the another complex molecule.

The mainstay of cancer treatment is chemotherapy [15] and the chief objective is to attain the maximum therapeutic damage to cancer cells with a minimal concentration of drugs [16,17]. Some metal ions are essential for cellular processes and their redox activity, reactivity and complexation ability towards organic substrates, and intracellular availability is tightly regulated. Even though they may be associated with various pathological disorders, including cancer, they are potential candidates as anticancer agents [18]. *Cisplatin*, *cis*-$[Pt(NH_3)_2Cl_2]$, is one of the most potent chemotherapy drugs and is widely used to treat many cancers [18-21]. However, *cisplatin* and some other platinum-based anticancer drugs (carboplatin and oxaliplatin) have several disadvantages, including side effects such as injury to renal tubular epithelial cells [20-22], nausea, vomiting [23], gastrointestinal toxicity [24], nephrotoxicity, elevated blood pressure and others [18,22,25,26], and some tumors are resistant to *cisplatin* [27,28]. Moreover, *cisplatin* has limited solubility in aqueous media [27,29,30] and responds to only a restricted spectrum of cancers [31,32]. Thus, there is scope to improve the toxicity [33,34] and effectiveness, along with a broader spectrum of action, elimination of side effects and increased solubility in future drugs [23]. Other strategies have already encompassed the development of water-soluble Pt(II) and multinuclear Pt(II) complexes, and complexes with bioactive donor molecules as secondary ligands [35-37] and the design the new anticancer agents with other central metal ions [27,38,39]. In particular, Pd(II) complexes have readily been chosen owing to their structural similarity to those containing Pt(II) ions [32,33,40,41]. These Pd(II) complexes were expected to exhibit lower kidney toxicity than *cisplatin* owing to the inability of the proteins in the kidney tubules to replace the tightly bound Pd(II) chelates with sulfhydryl groups [22,41,42]. In fact,

Pd(II) compounds exchange ligands 10^4-10^5 times faster than their Pt(II) analogs, i.e., Pt(II) complexes are thermodynamically and kinetically more stable than Pd(II) complexes [32,43]. The Pd(II) derivatives do not maintain their structural integrity in biological fluids for a long enough time to reach their pharmacological targets [26,32,44,45]. Nevertheless, several Pd(II) complexes containing *N*-, *N*,*N*- and *N,S*- aromatic ligands have shown promising anticancer activities [32,45,46,47].

Although it is generally accepted that DNA is the primary intracellular target of metal-based anticancer drugs, DNA-binding is chelate dependent. Changes in the structure of DNA upon binding with Pd(II) complexes have been reported, but a definite correlation between the structure and the mode of interaction has not been established [32,43,47]. Our research reported here deals with the synthesis of new Pd(II), Pt(II) and Ag(I) complexes based on (Δ)- and (Λ)-1,2–bis-(1H-benzimidazol-2-yl)-1,2-ethanediol (Δ-H_2bie and Λ-H_2bie) enantiomers in both the absence and presence of N,N-chelating ligands (bpy and phen) and PPh_3. The structures of the new complexes obtained are discussed in terms of their spectroscopic and other physical properties. In addition , we have examined their *in vitro* anticancer activity against human breast cancer (MDA-MB231) and ovarian cancer (OVCAR-8) cell lines as compared to *cisplatin*. Finally, we have used circular dichroism (CD) spectroscopy to study the DNA binding properties of the new complexes.

2. Experimental

2.1. Materials

All reagents and solvents were purchased from Alfa/Aesar and were used without further purification. All manipulations were performed under aerobic conditions. DMSO-d_6 was used for the NMR measurements, referenced against TMS. The [M(L)Cl_2] [M(II) = Pd, Pt; L = bpy, phen, PPh_3] complexes were prepared by the literature methods [48].

The human (MDA-MB231) cell line was obtained from the American Type Culture Collection (ATCC catalog number), while the human ovarian cancer (OVCAR-8) cell line was generously donated by Dr. Marie-Claude Beauchamp (MUHC, Lady Davis Institute, Jewish General Hospital, Montreal, QC, Canada). Cells were maintained in RPMI media from Wisent Bio Products, which was supplemented with Fetal Bovine Serum (FBS; 10%), HEPES (12 mL), L-glutamine (5 mL), gentamicin sulfate (500 µL), fungisone (250 µL) and ciprofloxacin (170 µL). All the bio-products used in the preparation of the media were purchased from Wisent Inc. The cells were grown in Corning cell cultured treated polystyrene flasks, which were placed in an incubator at 37 °C and at a CO_2 level of 5%. The media of each flask were changed when necessary and cell passaging was done between 85 and 95% confluence.

2.2. Measurements

Elemental analyses (C, H, N, Cl) were performed in the Microanalytical Unit, Department of Chemistry, Cairo University. Palladium and silver contents were determined by the reported methods [36]. Infrared spectra were recorded on a Nicolet 6700 Diamond ATR spectrometer in the 4000-200 cm^{-1} range. NMR spectra were measured on Varian Mercury 200, 300 and 500 MHz spectrometers, in DMSO d_6 using TMS as a reference. Mass spectra (ESI-MS) were recorded using LCQ Duo and double focusing MS25RFA instruments, respectively. Electronic spectra were obtained in DMF using a Hewlett-Packard 8453 spectrophotometer. Thermal

analysis measurements were made in the 20-1000 ^{o}C range at a heating rate of 20 ^{o}C min^{-1} using Ni and NiCo as references, on a on a TA instrument TGA model Q500 Analyzer TGA-50. Molar conductivity measurements were carried out at room temperature on a YSI Model 32 conductivity bridge. SEM analysis was performed using JEOL JSM 6510 lv.

2.3. Syntheses

(Δ)- and (Λ)-1,2–bis-(1H-benzimidazol-2-yl)-1,2-ethanediol (Δ-H_2bie and Λ-H_2bie)

A mixture of 1,2-phenylenediamine (10.00 g, 92.5 mmol) and D(-)- or L(+)-tartaric acid (6.94 g, 46.3 mmol) was dissolved in 4M HCl (200 mL). The reaction mixture was heated under reflux for 24 h. Upon cooling, green crystals of the chloride salt of the protonated ligand were obtained. These were dissolved in water (200 mL) and mixed with activated carbon under reflux for 2 h. The reaction mixture was treated with NH_4OH until neutralized and a white pprecipitate was obtained, which was filtered off and recrystallized from water-ethanol (1:1; V/V) to yield white needles or plates.

For Δ-H_2bie: Yield (25%). Elemental anal. Calcd. for ($C_{16}H_{14}N_4O_2$) C, 65.31; H, 4.76; N, 19.05%. Found: C, 65.30; H, 4.78; N, 19.01%.

For Λ-H_2bie: Yield (28%). Elemental anal. Calcd. for ($C_{16}H_{14}N_4O_2$) C, 65.31; H, 4.76; N, 19.05%. Found: C, 65.33; H, 4.75; N, 19.00%.

[Pd(L)$_2$]Cl$_2$.nH_2O (L = Δ-H_2bie, n = 3; L = Λ-H_2bie, n = 0)

An aqueous solution of $K_2[PdCl_4]$ (0.16 g, 0.5 mmol, 3 mL) was added to Δ-H_2bie or Λ-H_2bie (0.147 g, 0.5 mmol) in EtOH (15 mL). The suspension was stirred at 45 °C for 2 h and the

yellow-beige precipitate that formed was filtered off and washed with water, ethanol and air-dried**.**

For [Pd(Δ-H₂bie)₂]Cl₂.3H₂O: Yield: 73%. Elemental anal. Calcd.: C, 46.86; H, 4.15; Cl, 8.66; N, 13.67; Pd, 12.99 ($C_{32}Cl_2H_{34}N_8O_7Pd$); Found: C, 46.83; H, 4.08; Cl, 8.70; N, 13.54; Pd, 13.05%. Conductivity data (10^{-3} M in DMF): Λ_M = 189.2 ohm^{-1} cm^2 mol^{-1}.

For [Pd(Λ-H₂bie)₂]Cl₂: Yield: 61%. Elemental anal. Calcd.: C, 50.17; H, 3.52; Cl, 9.28; N, 14.63; Pd, 13.90 ($C_{32}Cl_2H_{28}N_8O_4Pd$); Found: C, 50.22; H, 3.78; Cl, 9.24; N, 14.45; Pd, 13.94%. Conductivity data (10^{-3} M in DMF): Λ_M = 188.4 ohm^{-1} cm^2 mol^{-1}.

[M(Λ-H₂bie)Cl(H₂O)]Cl.nH₂O (M = Pd, n = 2; M = Pt, n = 1)

A similar procedure to that for the [Pd(Λ-H_2bie)$_2$]Cl_2 analogue was employed. A bright yellow-orange (Pd) or yellow (Pt) precipitate was isolated after stirring for 24 h at room temperature.

For [Pd(Λ-H₂bie)(H₂O)Cl]Cl.2H₂O: Yield: 61%. Elemental anal. Calcd.: C, 36.54; H, 3.81; Cl, 13.51; N, 10.66; Pd, 20.25 ($C_{16}H_{20}Cl_2N_4O_5Pd$); Found: C, 36.28; H, 3.86; Cl, 13.44; N, 10.48; Pd, 20.56%. Conductivity data (10^{-3} M in DMF): Λ_M = 88.0 ohm^{-1} cm^2 mol^{-1}.

For [Pt(Λ-H₂bie)(H₂O)Cl]Cl.H₂O: Yield: 69%. Elemental anal. Calcd.: C, 32.21; H, 3.02; Cl, 11.91; N, 9.40 ($C_{16}H_{18}Cl_2N_4O_4Pt$); Found: C, 32.14; H, 3.11; Cl, 12.03; N, 9.55%. Conductivity data (10^{-3} M in DMF): Λ_M = 86.2 ohm^{-1} cm^2 mol^{-1}.

[Pt(Δ-H₂bie)₂](PF₆)₂.2H₂O

$K_2[PtCl_4]$ (0.05 g, 0.125 mmol) in water (3 mL) was added to Δ-H_2bie (0.0733 g, 0.25 mmol) in MeOH (10 mL), and the resulting solution was stirred at 40 °C for 24 h. A yellow precipitate was obtained upon adding saturated aqueous solution of NH_4PF_6 (2 mL). This precipitate was filtered off, washed with water, MeOH and air-dried. Yield: 83%. Elemental anal. Calcd.: C, 34.63; H, 2.89; N, 10.1 ($C_{32}H_{32}F_{12}N_8O_6P_2Pt$); Found: C, 34.53; H, 2.80; N, 10.02%. Conductivity data (10^{-3} M in DMF): Λ_M = 65.0 ohm^{-1} cm^2 mol^{-1}.

[M(L)(L')]Cl.nH_2O {M(II) = Pd, Pt; L = Δ-Hbie, Λ-Hbie; L' = bpy, phen}

To a stirred suspension of [Pd(L')Cl_2] (L' = bpy, phen; 1 mmol) in MeOH (20 mL), Δ-H_2bie or Λ-H_2bie (0.294 g, 1 mmol) in MeOH containing KOH (0.056 g, 1 mmol; 7 mL) was added dropwise with stirring over 30 min. The reaction mixture was warmed to 40 ^oC and allowed to stand for 36 h. After slow evaporation, a yellow-to-orange precipitate was isolated, which was filtered off, washed with water, MeOH and dried in *vacuo*.

For [Pd(bpy)(Δ-Hbie)]Cl.H_2O: Yield: 77%. Elemental anal. Calcd.: C, 51.24; H, 3.78; Cl, 5.83; N, 13.80; Pd, 17.47 ($C_{26}H_{23}ClN_6O_3Pd$); Found: C, 51.40; H, 3.84; Cl, 5.80; N, 13.66; Pd, 17.45%. Conductivity data (10^{-3} M in DMF): Λ_M = 84.0 ohm^{-1} cm^2 mol^{-1}.

For [Pd(bpy)(Λ-Hbie)]Cl: Yield: 70%. Elemental anal. Calcd.: C, 52.80; H, 3.55; Cl, 6.00; N, 14.22; Pd, 18.00 ($C_{26}ClH_{21}N_6O_2Pd$); Found: C, 52.61; H, 3.78; Cl, 5.83; N, 14.11; Pd, 18.11%. Conductivity data (10^{-3} M in DMF): Λ_M = 79.0 ohm^{-1} cm^2 mol^{-1}.

For [Pt(bpy)(Δ-Hbie)]Cl: Yield: 77%. Elemental anal. Calcd.: C, 45.92; H, 3.09; Cl, 5.22; N, 12.36 ($C_{26}ClH_{21}N_6O_2Pt$); Found: C, 45.78; H, 3.22; Cl, 5.01; N, 12.33%. Conductivity data (10^{-3} M in DMF): Λ_M = 89.0 ohm^{-1} cm^2 mol^{-1}.

For [Pt(bpy)(Λ-Hbie)]Cl: 70%. Elemental anal. Calcd.: C, 45.92; H, 3.09; Cl, 5.22; N, 12.36 ($C_{26}ClH_{21}N_6O_2Pt$); Found: C, 45.93; H, 3.10; Cl, 4.89; N, 12.21%. Conductivity data (10^{-3} M in DMF): Λ_M = 80.0 ohm^{-1} cm^2 mol^{-1}.

For [Pd(phen)(Δ-Hbie)]Cl: Yield: 69%. Elemental anal. Calcd.: C, 54.64; H, 3.42; Cl, 5.77; N, 13.66; Pd, 17.30 ($C_{28}ClH_{21}N_6O_2Pd$); Found: C, 54.52; H, 3.56; Cl, 5.74; N, 13.60; Pd, 17.32%. Conductivity data (10^{-3} M in DMF): Λ_M = 89.0 ohm^{-1} cm^2 mol^{-1}.

For [Pd(phen)(Λ-Hbie)]Cl: Yield: 64%. Elemental anal. Calcd.: C, 54.64; H, 3.42; Cl, 5.77; N, 13.66; Pd, 17.30 ($C_{28}ClH_{21}N_6O_2Pd$); Found: C, 54.63; H, 3.27; Cl, 5.76; N, 13.52; Pd, 17.24%.Conductivity data (10^{-3} M in DMF): Λ_M = 81.0 ohm^{-1} cm^2 mol^{-1}.

For [Pt(phen)(Δ-Hbie)]Cl: Yield: 65%. Elemental anal. Calcd.: C, 47.76; H, 3.00; Cl, 5.04; N, 11.94 ($C_{28}ClH_{21}N_6O_2Pt$); Found: C, 47.74; H, 3.01; Cl, 5.12; N, 11.83%. Conductivity data (10^{-3} M in DMF): Λ_M = 88.0 ohm^{-1} cm^2 mol^{-1}.

For [Pt(phen)(Λ-Hbie)]Cl: Yield: 60%. Elemental anal. Calcd.: C, 47.76; H, 3.00; Cl, 5.04; N, 11.94 ($C_{28}ClH_{21}N_6O_2Pt$); Found: C, 47.56; H, 3.09; Cl, 5.22; N, 11.56%. Conductivity data (10^{-3} M in DMF): Λ_M = 81.0 ohm^{-1} cm^2 mol^{-1}.

[M(PPh$_3$)(L)Cl].nH$_2$O (M(II) = Pd, L = Δ-Hbie, Λ-Hbie, n = 0; M(II) = Pt, L = Δ-Hbie, n = 1.5)

A suspension of [Pd(PPh$_3$)$_2$Cl$_2$] (0.0877 g, 0.125 mmol) in CH$_2$Cl$_2$ (10 mL) was mixed with Δ-H$_2$bie or Λ-H$_2$bie (0.037 g, 0.125 mmol) in MeOH containing KOH (0.007 g, 0.125 mmol; 4 mL). The reaction mixture was heated under reflux for 48 h. A yellow complex was obtained, which was filtered off, washed with CH$_2$Cl$_2$, CH$_3$OH and dried in *vacuo*.

For [Pd(Δ-Hbie)(PPh$_3$)Cl]: Yield: 80%. Elemental anal. Calcd. C, 58.54; H, 4.02; Cl, 5.09; N, 8.04; Pd, 15.27 ($C_{34}ClH_{28}N_4O_2PPd$); Found: C, 58.50; H, 4.15; Cl, 5.00; N, 8.07; Pd, 15.24 %. Conductivity data (10^{-3} M in DMF): Λ_M = 8.3 ohm^{-1} cm^2 mol^{-1}.

For [Pt(Δ-Hbie)(PPh$_3$)Cl].1.5H$_2$O: Yield: 76%. Elemental anal. Calcd. C, 50.22; H, 3.81; Cl, 4.37; N, 6.89 ($C_{34}ClH_{31}N_4O_{3.5}PPt$); Found: C, 50.14; H, 3.89; Cl, 4.26; N, 6.92%. Conductivity data (10^{-3} M in DMF): Λ_M = 7.5 ohm^{-1} cm^2 mol^{-1}.

For [Pd(PPh$_3$)(Λ-H$_2$bie)Cl]: Yield: 75%. Elemental anal. Calcd.: C, 58.54; H, 4.02; Cl, 5.09; N, 8.04; Pd, 15.27 ($C_{34}ClH_{28}N_4O_2PPd$); Found: C, 58.44; H, 4.00; Cl, 4.75; N, 8.04; Pd, 15.23 %. Conductivity data (10^{-3} M in DMF): Λ_M = 6.8 ohm^{-1} cm^2 mol^{-1}.

[Ag(L)$_2$]ClO$_4$ (L = Δ-H$_2$bie, Λ-H$_2$bie)

An aqueous solution of AgClO$_4$ (0.1036 g, 0.5 mmol; 2 mL) was added to Δ-H$_2$bie or Λ-H$_2$bie (0.1471 g, 0.5 mmol) in MeOH containing KOH (0.028 g, 0.5 mmol; 10 mL). The reaction

mixture was stirred in the dark at 50 °C for 4 h. The off-white precipitate that formed was filtered off, washed with warmed MeOH and dried in *vacuo*.

For [Ag(Δ-H₂bie)₂]ClO₄: Yield: 73%. Elemental anal. Calcd.: C, 48.27; H, 3.52; Ag, 13.58; N, 14.08; Cl, 4.46 ($AgC_{32}ClH_{28}N_8O_8$); Found: C, 48.21; H, 3.78; Ag, 13.44; N, 14.21; Cl, 4.40%. Conductivity data (10^{-3} M in DMF): Λ_M = 89.0 ohm^{-1} cm^2 mol^{-1}.

For [Ag(Λ-H₂bie)₂]ClO₄: Yield: 73%. Elemental anal. Calcd.: C, 48.27; H, 3.52; N, 14.08; Cl, 4.46 ($AgC_{32}ClH_{28}N_8O_8$); Found: C, 48.04; H, 3.51; N, 14.33; Cl, 4.34%. Conductivity data (10^{-3} M in DMF): Λ_M = 80.4 ohm^{-1} cm^2 mol^{-1}.

[Ag(L)(Δ-Hbie)] (L = phen, PPh_3)

A mixture of $AgClO_4$ (0.101 g, 0.5 mmol) in water (1 mL) and phen or PPh_3 (0.5 mmol) in MeOH (10 mL) was added to Δ-H_2bie (0.147 g, 0.5 mmol) in MeOH containing KOH (0.028 g, 0.5 mmol; 5 mL). The reaction mixture was stirred in the dark for 3 h at room temperature. The pale-yellow solid that formed was filtered off, washed with water, MeOH, Et_2O and dried in vacuo.

For [Ag(phen)(Δ-Hbie)]: Yield: 73%. Elemental anal. Calcd.: C, 52.01; H, 3.41; N, 13.00 ($C_{28}H_{22}AgN_6O_6$); Found: C, 51.82; H, 3.24; N, 12.83%. Conductivity data (10^{-3} M in DMF): Λ_M = 7.0 ohm^{-1} cm^2 mol^{-1}.

For [Ag(PPh$_3$)(Δ-Hbie)]: Yield: 66%. Elemental anal. Calcd. C, 61.38; H, 4.22; N, 8.44 ($C_{34}H_{28}AgN_4O_2P$); Found: C, 61.48; H, 4.30; N, 8.44%. Conductivity data (10^{-3} M in DMF): Λ_M = 5.0 ohm^{-1} cm^2 mol^{-1}.

[Ag(L)(Λ-H$_2$bie)]ClO$_4$ (L = bpy, PPh$_3$)

A mixture of $AgClO_4$ (0.05 g, 0.25 mmol) in water (0.5 mL) and bpy or PPh_3 (0.5 mmol) in MeOH (10 mL) was added to Λ-H_2bie (0.147 g, 0.5 mmol) in MeOH (10 mL). The reaction mixture was stirred in the dark for 3 h at room temperature. The resulting pale beige-yellow solid was filtered off, washed with water, MeOH, Et_2O and dried in vacuo.

For [Ag(bpy)(Λ-H$_2$bie)]ClO$_4$: Yield: 73%. Elemental anal. Calcd.: C, 47.45; H, 3.34; Cl, 5.40; N, 12.77 ($C_{26}H_{22}AgClN_6O_6$); Found: C, 47.41; H, 3.29; Cl, 5.30; N, 12.74%. Conductivity data (10^{-3} M in DMF): Λ_M = 99.0 ohm^{-1} cm^2 mol^{-1}.

For [Ag(PPh$_3$)(Λ-H$_2$bie)]ClO$_4$: Yield: 66%. Elemental anal. Calcd. C, 60.58; H, 4.31; Cl, 4.6; N, 5.27 ($C_{34}H_{29}AgClN_4O_6P$); Found: C, 60.50; H, 4.18; Cl, 4.61; N, 5.13%. Conductivity data (10^{-3} M in DMF): Λ_M = 92.0 ohm^{-1} cm^2 mol^{-1}.

2.4. Biological applications

2.4.1. Anticancer assays

Drug treatment: In all assays, drug stocks of 0.3125 x 10^{-2} to 100 µM were prepared by dissolution in DMSO.

***In vitro* growth inhibition essay:** To evaluate the biological activity of the drugs on cancer cells, the growth inhibiting effects on human breast cancer (MDAMB231) and human ovarian cancer (OVCAR-8) cell lines were examined *in vitro* and the results were compared against negative controls.

The human breast cancer (MDA-MB231) and human ovarian cancer (OVCAR-8) cell lines were grown to 80% confluence and then incubated in RPMI media onto 96-well plates (Corning Inc.) at a density of 3000-5000 cells per well (100 µL medium/well). They were allowed to attach for 24 h and then treated with a wide range of drugs, free ligands and their complexes, at concentrations ranging from 0.3125 x 10^{-2} to 100 µM. The treatment was designed to be carried out in triplicate over 5 days in the incubator. After treatment with the drugs, the cells were fixed with cold trichloroacetic acid (TCA) and dried as much as possible before staining with Sulforhodamine B (SRB; 50 µL, 0.4 g/100 mL) for at least 1 h at room temperature. Subsequently, the SRB well plates were rinsed with acetic acid (1%) and allowed to air dry overnight. Finally, the dye was dissolved in Tris-base (10 mM, pH 10–10.5; 200 µL) for 2-5 min on a shaking platform. The optical density for each well was recorded using a microplate reader (model 2550; Bio-Rad) at 492 nm [49]. Each drug concentration was run in triplicate in at least two independent experiments. The readings were analyzed using the GraphPad Prism program (GraphPad software, Inc.) and a sigmoidal dose-response curve was used to determine the 50% inhibitory concentration (IC_{50}) [49].

2.4.2. DNA binding

The circular dichroism spectral technique is useful in monitoring the conformational variations of DNA during complex-DNA interactions. The interactions of the new complexes with DNA were examined in 5 mM phosphate buffer – 50 mM NaCl (pH 7.2). The circulating tumor DNA (CT-DNA) shows a ratio of absorbance at 260 and 280 nm of about >1.86, indicating that the DNA was sufficiently free from protein [50]. The concentration of CT-DNA was determined from the absorption intensity at 260 nm, having a value of 6600 $(mol\,L^{-1})^{-1}cm^{-1}$. A stock solution was stored at 4 ºC and was used within one day. In addition, a stock solution (5 mM) of each complex was freshly prepared in water prior to use. Aliquots were added to a solution of CT-DNA (200 µM) freshly prepared in 5 mM phosphate buffer – 50 mM NaCl (pH 7.2) to achieve molar ratios of 0, 0.1, 0.21, 0.42, 0.63, 0.84 [complex]/[DNA] while keeping a total volume of 2 mL. The samples were incubated at 37 ºC for 24 h in the dark. All CD spectra of DNA and the DNA-complexes were recorded at 25 ºC in the 220–320 nm range. The absorption of free CT-DNA was canceled by adding equimolar CT-DNA to a pure buffer solution in the reference compartment and the resulting spectra were assumed to arise from the metal complexes and the DNA-metal complex aggregates. All solutions were mixed thoroughly and allowed to equilibrate for 60 min before data collection. While measuring the absorption spectra, an equal amount of DNA was added to both the complexes and the reference solutions to eliminate the CD contribution by CT-DNA, and the phosphate buffer – 50 mM NaCl (pH 7.2) was subtracted through base line correction.

3. Results and discussion

The syntheses of new complexes of Δ- and Λ-1,2–bis-(1H-benzimidazol-2-yl)-1,2-ethanediol (H_2bie) enantiomers with Pd(II), Pt(II) and Ag(I) ions are described in the Experimental section. The elemental analyses are in agreement with the assigned formulae. The molar conductivities (Λ_M) in DMF at room temperature suggest that the complexes are 1:1 electrolytes, except for $[Pd(L)_2]Cl_2$, (L = Δ-H_2bie, Λ-H_2bie) and $[Pt(\Delta\text{-}H_2bie)_2](PF_6)_2$, which are 1:2 electrolytes [51,52].

3.1. Vibrational spectra

Isele *et. al.* [53] have reported the potentiometric titrations of Λ-H_2bie. The first deprotonation takes place, for the alcoholic -OH hydrogen, at neutral pH (6–8), while the second is not observed below pH 10, indicating stabilization of the second –OH hydrogen atom, which may probably be attributed to hydrogen bond formation [53]. The IR spectra of the free ligands (Δ-H_2bie and Λ-H_2bie), show intramolecular H-bonding in the 2600–3450 cm^{-1} region as broad bands, which are weakened in the complexes, probably due to the participation of one of the two hydroxyl-O atoms in coordination. Both alcoholic groups become more acidic upon complexation. Some more intense hydrogen bonding is evidenced in the IR and Raman spectra of the complexes than in the free ligands owing to intermolecular H-bonding between the OH and NH groups [54].

The IR spectra of Δ-H_2bie and Λ-H_2bie show a medium band near 3055 cm^{-1} due to the ν(NH) stretch [54], while the bands near 3430 cm^{-1} belong to the ν(OH) stretches [54,55]. The medium-intense bands near 1597, 1317 and 1273 cm^{-1} (~1594, 1310 and 1277 cm^{-1} in the Raman spectra) in the free ligands are attributed to the ν(C=N), ν(C–N) and ν(C–O) stretches, respectively. Upon complexation, these bands are shifted to lower wavenumbers [54,55]. The out-of-plane C–

H bending appears at ~750 cm^{-1} as a strong band in the free ligands, while the weak bands in the 2815–2891 cm^{-1} range in the spectra of both the ligands and the complexes are assigned to the aliphatic ν(CH) vibrational stretches [54,55].

Mono-deprotonated complex formation can be achieved after addition of one equivalent of base (NaOH or KOH) per metal [53,54]. Thus, in these complexes, both Δ-$Hbie^-$ and Λ-$Hbie^-$ function as mono-negative bidentate ligands, coordinating the metal ions through the deprotonated hydroxyl-O and azomethine-N centers, forming five-membered chelate rings (Fig. 2). The ν(OH) stretch is shifted to a lower wavenumber (~3380 cm^{-1}), revealing the participation of one deprotonated hydroxyl-O atom in complexation, while the other remains uncoordinated [53-57]. The ν(C=N) stretches observed near 1600 and 1550 cm^{-1} (in the Raman spectra near 1590 and 1545 cm^{-1}) indicate the involvement of one azomethine-N atom in complexation, while the other plays no role in coordination [58,59]. The spectra of the ligands display bands near 3055 and 1280 cm^{-1} that are assigned to the imidazole ring NH stretch [60] and these remain more or less in the same position in the complexes, indicating no participation in coordination.

In the complexes, $[Pd(L)_2]Cl_2$ (L = Δ-H_2bie, Λ-H_2bie; Fig. 3), $[Pt(\Delta\text{-}H_2bie)_2](PF_6)_2$, $[M(\Lambda\text{-}H_2bie)Cl(H_2O)]Cl$ (M(II) = Pd, Pt), $[Ag(\Delta\text{-}H_2bie)_2]ClO_4$ and $[Ag(L')(\Lambda\text{-}H_2bie)]ClO_4$ (L' = bpy, PPh_3), the pH values of Δ-H_2bie or Λ-H_2bie were initially 7.5, but these were lowered to 5.5–6.1 upon addition of the corresponding metal salt, reflecting the inability of deprotonating the alcoholic -OH group [53,56,58,59]. The two ν(OH) modes, near 3200 and 3390 cm^{-1}, and the two ν(C=N) modes {near 1590 and 1540 cm^{-1} (~ 1595 and 1545 cm^{-1} in the Raman spectra)} indicate the involvement of one protonated hydroxy-OH and one azomethine-N atom in coordination, while the other groups do not participate in complex formation [54,56]. The ν(NH)

stretch remains more or less in the same position as in the free ligand, indicating no participation in coordination. The presence of the coordinated PPh_3 groups in [Pd(L-H)(PPh_3)Cl], [Ag(L-H)(PPh_3)] (L = Δ-H_2bie) and [Ag(Λ-H_2bie)(PPh_3)]ClO_4 is confirmed by the strong IR bands near 1095 and 750 cm^{-1}, which are attributed to the ν(P–C_{ph}) and δ(C–CH) vibrations, respectively [61].

The IR spectra of the [M(L)(L')]Cl (M(II) = Pd, Pt; L = Δ-Hbie or Λ-Hbie; L' = bpy, phen), [Ag(phen)(Δ-Hbie)] and [Ag(bpy)(Λ-H_2bie)]ClO_4 complexes display bands near 854, 841, 750 and 725 (in the case of bpy) and 1580, 1515, 1495 and 1420 cm^{-1} (in the case of phen), which are assigned to the γ(CH) vibrations of the coordinated phen or bpy ligands [62]. These bands are observed at higher wavenumbers compared with those for the free phen or bpy ligands, indicating their participation in complex formation [62]. Furthermore, the IR spectra of the complexes, [Ag(Λ-H_2bie)(L')]ClO_4 and [Ag$(L)_2$]ClO_4 (L = Δ-H_2bie, Λ-H_2bie; L' = bpy, PPh_3), exhibit bands near 1105 (strong) and 625 (medium) cm^{-1} due to the $\nu_3(T_2)$ and $\nu_4(T_2)$ modes of the uncoordinated T_d symmetry ClO_4^- ion, respectively [63]. The complex [Pt(Δ-H_2bie)$_2$]$(PF_6)_2$ displays a strong IR band at 865 cm^{-1} arising from the O_h symmetry $[PF_6]^-$ ion [64]. The Raman and IR spectra of the reported complexes show several bands in the 550–200 cm^{-1} region that are attributed to the ν(M-O), ν(M-N), ν(M-P) and ν(M-Cl) stretches [65,66].

3.2. NMR spectra

Assignments of the ^1H and ^{13}C NMR chemical shifts were obtained from the analysis of gCOSY (^1H), NOESY (^1H), ROESY (^1H), gHMBC (^1H-^{13}C) and gHSQC (^1H-^{13}C) spectra. In the ^1H NMR spectra of the free ligands, Δ-H_2bie and Λ-H_2bie, the aliphatic protons (H_1, $H_{1'}$) appear as doublets near δ 5.25 ppm, which change to singlets with considerable downfield shifts (δ 5.35-

5.85 ppm) in the complexes (see Fig.1 for the numbering scheme). The protons of the aliphatic OH and imidazole NH groups appear as doublets near δ 5.99 ppm and broad singlets at δ 12.38 ppm, respectively. The broad NH singlet indicates its fluxional behavior due to resonance through the N ⋯ C ⋯ N system [54,55,58,59], which is changed to HN-C=N in the complexes, and consequently, the NH proton appears as a sharp signal in comparison to that for the free ligand [54,55]. The aromatic protons appear as doublets (H_4, $H_{4'}$, H_7, $H_{7'}$) and triplets (H_5, $H_{5'}$, H_6, $H_{6'}$) at δ 7.15 and 7.50 ppm, respectively (Fig. 4, Table 1).

In the spectra of the complexes prepared in the presence of base (1:1; M: KOH), the resonance of the hydroxy protons at δ 5.99 ppm is absent , while a new singlet appears near δ 6.07 ppm, indicating deprotonation of one –OH group upon coordination to the metal ion, while the second –OH group remains uncoordinated [67]. The intensity of the new –OH singlet is less than that of the doublet in the free ligand, which may be attributed to the involvement of the uncoordinated –OH group in H-bonding with the solvent [56]. The signals for the imidazole NH proton (δ 12.40–13.8 ppm), the aromatic protons (δ 7.17–8.0 ppm) and aliphatic protons are all shifted downfield [62]. This feature may be attributed to a decrease in the electron density in the imidazole ring upon complexation through the azomethine nitrogen atom [68,69]. In addition, two doublets (near δ 7.80, 8.00 ppm) and two triplets (near δ 7.15, 7.5 ppm) are observed for the aromatic protons, indicating coordination of the metal ion *via* a deprotonated hydroxyl-O atom and a close azomethine-N atom in a mono-negative bidentate manner, while the other side remains uncoordinated (Fig. 4c) [53-55].

In the spectra of the complexes, $[Pd(L)_2]Cl_2$ (L = Δ-H_2bie, Λ-H_2bie), $[Pt(\Delta\text{-}H_2bie)_2](PF_6)_2$, $[M(\Lambda\text{-}H_2bie)Cl(H_2O)]Cl$ (M = Pd, Pt), $[Ag(\Delta\text{-}H_2bie)_2]ClO_4$ and $[Ag(L')(\Lambda\text{-}H_2bie)]ClO_4$ (L' = bpy, PPh_3), two doublets and two triplets for the aromatic protons, and two singlets for the hydroxy

protons are observed together with clear downfield shifts of the aliphatic, imidazole NH and aromatic proton resonances. These observations support coordination of Δ-H_2bie and Λ-H_2bie in a neutral bidentate manner, through one protonated hydroxyl-OH group and a nearby azomethine-N atom [56].

For the complexes $[Pd(L)_2]Cl_2$, $[Ag(L)_2]ClO_4$ (L = Δ-H_2bie, Λ-H_2bie) and $[Pt(\Delta\text{-}H_2bie)_2](PF_6)_2$, *cis* and/or *trans* isomers are possible. Their ^{1}H NMR spectra reveal the presence of only one resonance for each of the two equivalent protons, suggesting the presence of a *trans* configuration, except for $[Pt(\Delta\text{-}H_2bie)_2](PF_6)_2$ and $[Pd(\Lambda\text{-}H_2bie)_2]Cl_2$ (Figs. 2 and 5) which have two equivalent signals for each proton, confirming their presence in a *cis*-configuration [70].

In the ^{13}C NMR spectra of free Δ-H_2bie and Λ-H_2bie, there are eight resonances near δ 71.6, 156.29, 134.73, 122.18, 119.04, 112.09, 121.6 and 122.20 ppm, corresponding to C(1), C(2), C(4), C(5), C(6), C(7) and C(8), respectively (Table 2). In the complexes, $[Pd(\Delta\text{-}H_2bie)_2]Cl_2$, $[Pt(\Delta\text{-}H_2bie)_2](PF_6)_2$ and $[Pd(\Lambda\text{-}H_2bie)Cl(H_2O)]Cl$, the carbon atoms adjacent to the coordination centers C(1), C(2) and C(8) are shifted to ~ δ 69.80, 153.75 and 132.10 ppm, respectively, indicating the coordination of both protonated hydroxyl-O and azomethine-N atoms in a neutral bidentate manner [71]. In addition, the spectra of $[Pd(\Lambda\text{-}H_2bie)_2]Cl_2$ and $[Pt(\Delta\text{-}H_2bie)_2](PF_6)_2$ show two resonances for each carbon atom, supporting the *cis*-configuration that was concluded from their ^{1}H NMR spectra [72].

Upon comparing the ^{13}C NMR spectra of the complexes [M(phen)(Δ-Hbie)]Cl (M = Pd, Pt) and [Pd(phen)(Λ-Hbie)]Cl to those of ligands, there are clear shifts in the C(1), C(2) and C(8) resonances, together with only small shifts for C(3) and C(7) being observed, indicating the participation of one deprotonated -OH group and the nearest azomethine nitrogen atom in coordination [68].

Finally, the ^{31}P NMR spectra of [Pd(PPh_3)(Δ-Hbie)Cl], [Pd(PPh_3)(Λ-Hbie)Cl] and [Ag(PPh_3)(Δ-Hbie)] exhibit one signal near δ 52 ppm, indicating the presence of one PPh_3 group in these complexes [73]. The ^{31}P NMR spectrum of [Pt(Δ-H_2bie)$_2$](PF_6)$_2$ has one signal at δ 28.7 ppm, revealing the presence of the uncoordinated $[PF_6]^-$ ion [74].

3.3. Electronic spectra

The electronic spectra of the complexes were recorded in DMSO in the 200-800 nm range. The spectra of Δ-H_2bie and Λ-H_2bie in DMSO show absorption bands near 240 and 300 nm due to n → π* and π → π * transitions, respectively [65]. The electronic spectra of the diamagnetic Pd(II) and Pt(II) complexes display bands near 470 and 320 nm attributable to $^1A_{1g} \rightarrow {}^1B_{1g}$ and $^1A_{1g} \rightarrow {}^1E_{1g}$ transitions associated with the square-planar configuration [52,54]. The absorption band near 375 nm in the [M(L)(Δ-Hbie)]Cl and [M(L)(Δ-Hbie)]Cl (M(II) = Pd, Pt; L = bpy, phen) complexes is assigned to a mixture of charge-transfer transitions from a M(II) d-orbital to the π*-orbital of bpy or phen [49].

3.4. Mass spectra

The mass spectra of the complexes exhibit fragmentation patterns that reflect the stepwise loss of the ligands. The mass spectra of the complexes, [Pd(Δ-H_2bie)$_2$]Cl_2 and [Pd(Λ-H_2bie)$_2$]Cl_2 (Fig 6), display signals at *m/z* 693.99 (Calcd. 694.4) and 1388.9 (Calcd. 1388.4) with 10 and 12% abundance, in agreement with the molecular ions of the complexes, $[Pd(\Delta\text{-}H_2bie)_2]^+$ and $[Pd_2(\Lambda\text{-}H_2bie)_4]^+$, respectively [75]. The fragmentation pattern of the former complex indicates the formation of a $[Pd(\Delta\text{-}H_2bie\text{-}C_6H_4)_2]^+$ fragment at *m/z* 542.7 (Calcd. 542.4), while that of the latter indicates the loss of Λ-H_2bie, Λ-H_2bie, Pd, C_6H_4 and $C_6H_6N_2$ fragments at *m/z* 1095.2 (Calcd.

1094.8) {[$Pd_2(\Lambda\text{-}H_2bie)_3]^+$}, 801.3 (Calcd. 800.8) {[$Pd_2(\Lambda\text{-}H_2bie)_2]^+$}, 695.3 (Calcd. 694.4) {[$Pd(\Lambda\text{-}H_2bie)_2]^+$}, 618.8 (Calcd. 618.4) {[$Pd(\Lambda\text{-}H_2bie\text{-}C_6H_4)_2]^+$} and 512.5 (Calcd. 512.4) {[$Pd(\Lambda\text{-}H_2bie\text{-}C_6H_6N)_2]^+$} [68]. The mass spectrum of [$Pt(\Delta\text{-}H_2bie)_2](PF_6)_2$, shows the first molecular ion peak at *m/z* 783.6 (Calcd. 783.0) with 81% abundance, corresponding to [$Pt(\Delta\text{-}H_2bie)_2]^+$. The peaks at *m/z* 707.3 (Calcd. 707.1) and 489.3 (Calcd. 489.0) represent the fragments, [$Pt(\Delta\text{-}H_2bie)(\Delta\text{-}H_2bie\text{-}C_6H_4)]^+$ and [$Pt(\Delta\text{-}H_2bie)]^+$, respectively [71,76]. The spectra of the complexes [$Pd(\Lambda\text{-}H_2bie)Cl(H_2O)$]Cl and [$Pt(\Lambda\text{-}H_2bie)Cl(H_2O)$]Cl shows ion peaks at *m/z* 400.8 (Calcd. 400.4) and 490.0 (Calcd. 489.0) with 11 and 12.3% abundance, representing the molecular ions [$Pd(\Lambda\text{-}H_2bie)]^+$ and [$Pt(\Lambda\text{-}H_2bie)]^+$, respectively. The former one shows one more peak at *m/z* 294.8 (Calcd. 294.4), corresponding to the [$Pd(\Lambda\text{-}H_2bie\text{-}C_6H_6N_2)]^+$ fragment.

The mass spectra of the complexes, [Pd(bpy)(Δ-Hbie)]Cl, [Pd(bpy)(Λ-Hbie)], [Pd(phen)(Δ-Hbie)] and [Pd(phen)(Λ-Hbie)] exhibit molecular ion peaks at *m/z* 555.1 (Calcd. 555.4), 554.99 (Calcd. 555.4), 579.4 (Calcd. 579.4) and 579.3 (Calcd. 579.4) with 100, 42, 6.7 and 12.8% abundance, in agreement with the molecular ions, [Pd(bpy)(Δ-Hbie)]$^+$, [Pd(bpy)(Λ-Hbie)]$^+$, [Pd(phen)(Δ-Hbie)]$^+$ and [Pd(phen)(Λ-Hbie)]$^+$, respectively. The fragmentation patterns indicate the loss of a C_6H_5N fragment from {[Pd(bpy)(Δ-Hbie-C_6H_5N)]$^+$ at *m/z* 464.2 (Calcd. 464.4)}, while those of the phen complex show the loss of C_6H_4 fragments from {[Pd(phen)(Δ-Hbie-C_6H_4)]$^+$ at *m/z* 503.6 (Calcd. 503.4) and [Pd(phen)(Λ-Hbie-C_6H_4)]$^+$ 503.5 (Calcd. 503.4), respectively}. On the other hand, the mass spectra of the complexes, [Pt(bpy)(Δ-Hbie)]Cl, [Pt(bpy)(Λ-Hbie)], [Pt(phen)(Δ-Hbie)] and [Pt(phen)(Λ-Hbie)] (Fig. 6), show signals at *m/z* 644.3 (Calcd. 644.0), 645.0 (Calcd. 644.0), 668.3 (Calcd. 668.0) and 668.6 (Calcd. 668.0) with 66, 5.4, 26 and 10% abundance, in agreement with the molecular ions, [Pt(bpy)(Δ-Hbie)]$^+$,

$[Pt(bpy)(\Lambda\text{-Hbie})]^+$, $[Pt(phen)(\Delta\text{-Hbie})]^+$ and $[Pt(phen)(\Lambda\text{-Hbie})]^+$, respectively. The fragmentation patterns indicate the loss of C_6H_4 and C_6H_5N fragments from the second and fourth complexes, i.e., $[Pt(bpy)(\Lambda\text{-Hbie-}C_6H_4)]^+$ at *m/z* 568.7 (Calcd. 568.0) and $[Pt(phen)(\Lambda\text{-Hbie-}C_6H_5N)]^+$ at *m/z* 485.9 (Calcd. 486.0), respectively.

The mass spectra of the complexes $[Pd(PPh_3)(\Delta\text{-Hbie})Cl]$, $[Pd(PPh_3)(\Lambda\text{-Hbie})Cl]$ and $[Pt(PPh_3)(\Delta\text{-Hbie})Cl]$ show signals at *m/z* 661.8 (Calcd. 661.4), 663.3 (Calcd. 661.4) and 750.3 (Calcd. 750.0) with ~10% abundance due to the molecular ions, $[Pd(PPh_3)(\Delta\text{-Hbie})]^+$, $[Pd(PPh_3)(\Lambda\text{-Hbie})]^+$ and $[Pt(PPh_3)(\Delta\text{-Hbie})]^+$. The spectrum of the former complex exhibits one more peak at *m/z* 584.3 (Calcd. 585.4), corresponding to the $[Pd(PPh_3)(\Delta\text{-Hbie-}C_6H_4)]^+$ fragment.

The mass spectra of $[Ag(\Delta\text{-}H_2bie)_2]ClO_4$ and $[Ag(\Lambda\text{-}H_2bie)_2]ClO_4$ show signals at *m/z* 696.4 (Calcd. 696.0) and 697.1 (Calcd. 696.0) with 21 and 15.3% abundance, corresponding to $[Ag(\Delta\text{-}H_2bie)_2]^+$ and $[Ag(\Lambda\text{-}H_2bie)_2]^+$, respectively. The former complex show two more signals at *m/z* 514.3 (Calcd. 514.0) and 402.2 (Calcd. 402.0), corresponding to the $[Ag(\Delta\text{-}H_2bie)(\Delta\text{-}H_2bie\text{-}C_6H_5N)]^+$ and $[Ag(\Delta\text{-}H_2bie)]^+$ fragments, respectively, while the latter shows one peak at *m/z* 402.9 (Calcd. 402) due to the $[Ag(\Lambda\text{-}H_2bie)]^+$ fragment.

The mass spectrum of $[Ag(PPh_3)(\Delta\text{-Hbie})]$ (Fig. 6) exhibits the first signal at *m/z* 664.1 (Calcd. 663.0), corresponding to $[Ag(PPh_3)(\Delta\text{-Hbie})]^+$. A stepwise ligand loss reveals signals at *m/z* 400.8 (Calcd.400.0) and 369.8 (Calcd. 370.0), corresponding to $[Ag(PPh_3)(\Delta\text{-Hbie-}C_{16}H_{14}N_3O)]^+$ and $[Ag(PPh_3)]^+$ fragments, respectively [68]. The mass spectrum of $[Ag(bpy)(\Lambda\text{-}H_2bie)]ClO_4$ (Fig. 3.2.4.11), exhibits a signal at *m/z* 559.1 (Calcd. 558.0) with 65.5% abundance, corresponding to $[Ag(bpy)(\Lambda\text{-}H_2bie)]^+$, while that of $[Ag(PPh_3)(\Lambda\text{-}H_2bie)]ClO_4$ shows three

peaks at *m/z* 665.2 (Calcd. 664.0), 634.6 (Calcd. 634.0) and 371.2 (Calcd. 370.0), due to $[Ag(PPh_3)(\Lambda\text{-}H_2bie)]^+$, $[Ag(PPh_3)(\Lambda\text{-}H_2bie\text{-}2NH)]^+$ and $[Ag(PPh_3)]^+$ fragments, respectively [68,72].

3.5. Thermal measurements

According to the TGA curves, the observed mass-loss stages arise from the elimination of hydrated water, coordinated water and/or Cl_2, and elimination of PPh_3 followed by decomposition of the Δ-H_2bie, Λ-H_2bie, Δ-$Hbie^-$ or Λ-$Hbie^-$ moiety {or decomposition of Δ-H_2bie, Λ-H_2bie, Δ-$Hbie^-$ or Λ-$Hbie^-$ followed by loss of phen or bpy}. The decomposition of the Δ-H_2bie, Λ-H_2bie, Δ-$Hbie^-$ or Λ-$Hbie^-$ moiety takes place through the breakdown of the weak C_6H_4-N, C_6H_4-NH, C(1)-N, C(1')-N, C(1)-O or C(1')-O hetero bonds [61,77-79]. All the complexes show thermal stability up to 200 ^oC. The complexes of both Δ-H_2bie and Λ-H_2bie or Δ-$Hbie^-$ and Λ-$Hbie^-$ enantiomers display the same thermal behavior with the same metal ion and/or the second chelating agent (bpy, phen or PPh_3). The thermograms of the complexes, $[Ag(\Delta\text{-}Hbie)(PPh_3)]$ and $[Ag(\Lambda\text{-}H_2bie)(PPh_3)\}ClO_4$, do not reflect the same behavior, based on the difference in the chelation modes of Δ-$Hbie^-$ and Λ-H_2bie, respectively. The weight loss observed below ~ 130 ºC is due to dehydration as the colors of the complexes changed from pale to a deeper one [62,79].

The thermogram of $[Pd(\Delta\text{-}H_2bie)_2]Cl_2.3H_2O$ shows the first weight loss between 50 and 175 ºC, arising from the release of three hydrated water molecules (Calcd. 6.6, Found 6.7%). The second endothermic decomposition step occurs between 176 and 415 ºC, and is attributed to the loss of

two C_6H_4 and Cl_2 species (Calcd. 27.2, Found 27.0%), while the third and fourth endothermic inflections (416-620 and 621-910 ºC) may arise from the elimination of two $C_8H_7N_3O$ (Calcd. 39.3, Found 39.3%) and two $C_2H_2N_2O_{1/2}$ (Calcd. 15.1, Found 15.3%) fragments, respectively, leaving 14.9% for the PdO residue [80,81].

The TGA thermogram of $[Pt(\Delta\text{-}H_2bie)_2](PF_6)_2.2H_2O$ is characterized by three steps in the 50–180, 181–389 and 390-700 ºC regions that are due to the release of hydrated water (Calcd. 3.3, Found 3.3%), $2PF_6$, $4C_6H_4$, N_2 and H_2 species (Calcd. 55.0, Found 55.4%) and {two $C_4H_4N_3O_2$} (Calcd. 21.3, Found 21.3%) fragments, respectively, leaving a PtO residue (18.1%) [80,81].

The complex $[Pd(\Lambda\text{-}H_2bie)_2]Cl_2$ (Fig. 7) shows weight losses in the 55– 450 and 451–590 ºC regions that may correspond to the release of Cl_2, N_2 and $4C_6H_5N$ (Cacld. 60.5, Found 60.3%) and $2C_3H_4NO$ and O_2 (Calcd. 20.4, Found 20.6%) species, respectively, leaving a mixed Pd(II) oxide and carbide residue at 650 ^oC (19.8%). The thermogram of $[Pd(\Lambda\text{-}H_2bie)(H_2O)Cl]Cl.2H_2O$ consists of three steps in the 62–117, 200–322 and 324-526 ºC regions. These are assigned to the elimination of {½ Cl_2 and hydrated water} (Calcd. 13.6, Found 13.7%), {coordinated water, ½ Cl_2, N_2 and H_2} (Calcd. 15.9, Found 16.1%) and $2C_6H_4$ (Calcd. 28.9, Found 29.0) fragments, respectively, leaving a palladium nitride, carbide and oxide residue (26.4%). On the other hand, the thermogram of $[Pt(\Lambda\text{-}H_2bie)(H_2O)Cl]Cl.H_2O$ shows four decomposition steps in the 45-180, 181-500, 501-812 and 813-900 ^oC regions, which may be attributed to the elimination of hydrated water (Calcd. 3.0, Found 3.2%), coordinated water and Cl_2 (Calcd. 14.9, Found 14.5%), C_6H_4 (Calcd. 12.8, Found 12.6%) and C_6H_5N (Calcd. 15.3, Found 15.5%) fragments, respectively, leaving a Pt(II) residue (45.5%) [72].

The thermogram of $[Pd(bpy)(\Delta\text{-}Hbie)]Cl.H_2O$ (Fig. 7) indicates the first weight loss between 38

and 145 ^{o}C due to the release of a hydrated water molecule (Calcd. 3.0, Found 3.2%). There are five more endothermic TG inflections in the 146-225, 226-325, 326-562, 563-615 and 616–970 ºC regions, which arise from the elimination of ½ Cl_2 (Calcd. 5.8, Found 5.7%), $2C_6H_5N$ (Calcd. 27.4, Found 27.0%), ½ bpy (Calcd. 12.8, Found 12.7%), {½ bpy, N_2, ½ O_2 and $1.5H_2$} (Calcd. 20.5, Found 20.2%) and C_4H_2N (Calcd. 10.5, Found 10.6%) species, respectively, leaving a PdO residue (20.1%) [82]. The thermogram of [Pd(bpy)(Λ-Hbie)]Cl is characterized by three steps in the 280–333, 334-428 and 742–790 ºC regions. These are assigned to the elimination of {½ Cl_2, ½ bpy, C_6H_5N} (Calcd. 34.6, Found 34.9%), {½ bpy, C_6H_5N} (Calcd. 28.6, Found 28.2%) and ½ N_2 (Calcd. 2.4, Found 2.3%) fragments, respectively, leaving a residue (27.7%). The thermogram of [Pd(phen)(Δ-Hbie)]Cl shows three TG inflections in the 55–210, 211–512 and 513-790 ºC regions, which are attributed to the elimination of ½ Cl_2 (Calcd. 5.8, Found 5.4%), {phen, $2C_6H_4$, ½ N_2 and ½ H_2 species} (Calcd. 56.4, Found 55.8%) and a $C_4H_4N_3O$ fragment (Calcd. 17.9, Found 18.3%), leaving a PdO residue (17.3%) [72].

The TG of [Pd(phen)(Λ-Hbie)]Cl has two endothermic decomposition steps in the 296–320 and 340–444 ºC regions, assigned to the loss of {½ Cl_2 and C_6H_4 fragments} (Calcd. 18.1, Found 18.3%) and {phen, $C_6H_5N_2$, ½ N_2 and ½ H_2 species} (Calcd. 48.8, Found 49.1%), respectively, leaving a residue (35.4%) [77].

The thermogram of [Pd(Δ-Hbie)$(PPh_3)_2$Cl] shows the first step weight loss between 218 and 400 ^{o}C that corresponds to the release of ½ Cl_2 and PPh_3 and $2C_6H_4$ fragments (Calcd. 64.5, Found 65.0%). The second decomposition occurs between 401 and 828 ^{o}C due to the elimination of a $C_3H_4N_3O$ fragment (Calcd. 14.1, Found 13.8%) [53], leaving a PdO residue (21.6%). The thermogram of [Pt(Δ-Hbie)$(PPh_3)_2$Cl]$1.5H_2O$ shows TG inflections in the 45-180, 181-230, 231-

521, 522-800 and 800–900 °C regions. These weight losses arise from the release of hydrate water (Calcd. 3.3, Found 3.5%), {½ Cl_2, Ph} (Calcd. 13.8, Found 13.5%), {½ N_2, ½ H_2, PPh_2} (Calcd. 24.6, Found 24.9%), {2C_6H_5N, H_2, ½ O_2} (Calcd. 24.6, Found 24.7%) and C_4HN (Calcd. 6.3, Found 6.6%) fragments, respectively, leaving a PtO residue (26.0%) [75].

The thermogram of [$Pd(PPh_3)_2$(Λ-H_2bie)]Cl, is characterized by only one endothermic step in the 270–488 °C region due to the elimination of ½ Cl_2, PPh_3 and $C_6H_5N_2$ fragments (Calcd. 57.8, Found 58.0%), leaving a Pd(II) residue at 650 °C (36.4%) [75]. The thermogram of [Ag(Δ-H_2bie)$_2$]ClO_4 shows two endothermic TG inflections in the 200–510 and 511–620 °C regions. These arise from the release of {½ Cl_2, 2O_2, C_6H_5N and 3C_6H_4} (Calcd. 52.6, Found 52.9%) and {2$C_3H_5N_2O$ and ½ N_2} (Calcd. 23.1, found 23.4) fragments, respectively [83], leaving a residue of silver carbide, oxide and azide (23.7%). On the other hand, the thermogram of [Ag(Δ-H_2bie)$_2$]ClO_4 (Fig. 7), shows three TG inflections in the 200-295, 296-425 and 426-520 °C regions. These weight losses may arise from the release of {½ Cl_2, 2O_2, C_6H_5N} (Calcd. 23.9, Found 24.0%), {$C_6H_5N_2$, N_2, H_2} (Calcd. 17.0, Found 17.1%) and 2C_6H_4 (Calcd. 19.1, found 19.5) fragments, respectively [80], leaving a residue of silver oxide (38.6%) [75].

The thermogram of [$Ag(PPh_3)$(Δ-Hbie)] shows three TG inflections in the 205-315, 316-520 and 521-720 °C ranges, indicating the release of {PPh_3 and 2C_6H_4} (Calcd. 62.4, Found 62.6%), {$C_2H_5N_2$, ½ O_2, ½ N_2, H_2} (Calcd. 13.3, Found 13.8%) and {C_2N, ¼ O_2} (Calcd. 6.9, Found 7.1%) species, respectively, leaving the Ag_2O residue (17.5%). The TG thermogram of [$Ag(PPh_3)$(Λ-H_2bie)]ClO_4 (Fig. 7) displays two TG weight losses. The first between 190 and 310 °C may arise from the release of {½ Cl_2, 2O_2, $C_6H_5N_2$, ½ N_2, ½ H_2, PPh_3} (Calcd. 63.1, Found 63.0%), while the second (311-900 °C) is assigned to the release of {C_6H_4, $C_2H_2O_{1.5}$} (Calcd. 16.5, Found 16.8%) fragments [80], leaving a residue of silver oxide.

Finally, the TG thermogram of [Ag(phen)(Δ-Hbie)] shows the first endothermic weight loss step between 196 and 310 ^{o}C, corresponding to the release of $C_6H_5N_2$, ½ N_2, ½ H_2 (Calcd. 20.7, Found 20.6%). The second decomposition step occurs between 311 and 545 ^{o}C, which is attributed the loss of phen and C_6H_4 fragments (Calcd. 44.1, Found 43.6%). The third TG inflection between 546 and 607 ^{o}C is attributed to the loss of a C_2H_2NO fragment (Calcd. 9.6, Found 10.2%). The last step between 608 and 800 ^{o}C, is due to the release of $C_2O_{1/5}$ (Calcd. 5.5, Found 5.1%), leaving a Ag_2O residue (24.7%) [72,80].

3.6. Biological applications

In the field of pharmacology, the most important advances have been the proven efficacy of chiral or enantiopure drugs. Single enantiopure drugs have been shown to be better drugs, i.e. safer and more potent, than racemate drugs [84]. Chiral drugs are assumed to be therapeutically active as most of the bio-targets of drugs are chiral in nature. Therefore, considerable attention has been paid to the design and construction of chiral molecules that are versatile in occupying the active site, possess a metal-binding domain and have a bioactive organic functionality (pharmacophore), which pre-orients the molecule as a drug entity and reduces the toxicity parameters [53]. The introduction of chirality enhances the pharmacological behavior of a metal complex by adopting a specific conformation and a target selective binding affinity for DNA (as DNA itself exists in nature only in one chiral form) [85]. The design of metal-based pharmaceuticals depends on the donor framework, the choice of metal ion and its oxidation state [86]. The donors can significantly alter the biological properties by modifying reactivity or substitution inertness. Tailored, multifunctional donors introduced into metal-based medicinal agents facilitate metal ion redistribution, limit their adverse effects upon overloading and

inhibiting selected metallo-enzymes [87]. Therefore, chiral metal complexes have a promising future as robust chemotherapeutic agents in medicinal inorganic chemistry.

3.6.1. Anticancer studies

As stated earlier, the main objective of this research was to obtain new pairs of enantiomeric chiral, Δ-1,2–bis-(1H-benzimidazol-2-yl)-1,2-ethanediol (Δ-H_2bie) and Λ-1,2–bis-(1H-benzimidazol-2-yl)-1,2-ethanediol (Λ-H_2bie) complexes, with low cytotoxicity and high efficacy against the human breast (MDA-MB231) and ovarian cancer (OVCAR-8) cell lines, which unfortunately have high incidence rates throughout the world. Chirality is an attractive prospect, because of its ability to enhance the pharmacological uptake of the drug entity by adopting a specific conformation and stereo-selective binding with the DNA molecular target [88].

To evaluate the anticancer efficacy of the pairs of enantiomeric Δ-H_2bie and Λ-H_2bie complexes, the *in vitro* anticancer activities of free Δ-H_2bie and Λ-H_2bie and their complexes, [Pd(Δ-H_2bie)$_2$]Cl_2, [Pt(Δ-H_2bie)$_2$]$(PF_6)_2$, [Pd(bpy)(Δ-Hbie)]Cl, [Pd(phen)(Δ-Hbie)]Cl, [Pt(bpy)(Δ-Hbie)]Cl, [Pt(phen)(Δ-Hbie)]Cl, [Pd(Δ-Hbie)(PPh_3)Cl], [Pt(Δ-Hbie)(PPh_3)Cl], [Ag(Δ-H_2bie)$_2$]ClO_4, [Ag(phen)(Δ-Hbie)], [Ag(PPh_3)(Δ-Hbie)], [Pd(bpy)(Λ-Hbie)]Cl, [Pd(phen)(Λ-Hbie)]Cl, [Pt(bpy)(Λ-Hbie)]Cl, [Pt(phen)(Λ-Hbie)]Cl, [Pd(Λ-H_2bie)$_2$]Cl_2, [Pd(Λ-Hbie)(PPh_3)Cl], [Pd(Λ-H_2bie)(H_2O)Cl]Cl, [Pt(Λ-H_2bie)(H_2O)Cl]Cl, [Ag(Λ-H_2bie)$_2$]ClO_4, [Ag(bpy)(Λ-H_2bie)]ClO_4 and [Ag(PPh_3)(Λ-H_2bie)]ClO_4, were tested for their inhibitory effects on the cell growth proliferation of the human breast (MDA-MB231) and ovarian cancer (OVCAR-8) cell lines using *cisplatin* as a reference compound. The cell growth proliferation was evaluated by RPMI assays. The final IC_{50} values for cell growth proliferation after 24 h of incubation with

free Δ-H_2bie and Λ-H_2bie, and their complexes, for MDA-MB231 and OVCAR-8 cell lines are reported in Tables 3 and 4, and Fig. 8. There was no great difference in cytotoxicity between the two enantiomers reported earlier for the pair of enantiomeric complexes, *cis*-[Pt(R(–)HBB)$_2$Cl$_2$] and *cis*-[Pt(S(+)HBB)$_2$Cl$_2$] (HBB = 2-α-hydroxybenzylbenzimidazole) in their activity against the human breast cancer (MCF-7) and HeLa cervix cancer cell lines [89].

The fact that the complexes of the Δ-H_2bie enantiomer were more active against the studied cell lines is further supported by the *in vitro* cytotoxicity of the pair of enantiomeric complexes, [Pt(R,R-eap)Cl$_2$] and [Pt(S,S-eap)Cl$_2$] (eap = N,N-diethyl-2,4-pentanediamine), against murine leukemia and human bladder tumor cells. The R,R- enantiomer was more active against leukemia cells, while no significant difference in activity was reported against the bladder tumor cell line [89]. It is clear that the cytotoxicity of Δ-H_2bie and Λ-H_2bie is notably low in both studied cell lines, with IC_{50} values greater than 100 μM, indicating that the cytotoxic effect is due the metal complexes. The order for the cytotoxic activity of the complexes is Ag(I)-PPh_3 > Ag(I)-phen > Pt(II)-phen > Pd(II)-phen > Ag(I)-bpy > Ag(I) > Pt(II)-bpy > Pd(II)-bpy > Pt(II)-PPh_3 > Pd(II)-PPh_3 > Pd(II) > Pt(II) for the central metal ion [91]. The [Ag(PPh_3)(Λ-H_2bie)]ClO_4, [Ag(PPh_3)(Δ-Hbie)], [Ag(phen)(Δ-Hbie)], [Pt(phen)(Δ-Hbie)]Cl, [Pd(phen)(Δ-Hbie)]Cl, [Pt(phen)(Λ-Hbie)]Cl, [Pd(phen)(Λ-Hbie)]Cl and [Ag(bpy)(Λ-H_2bie)]ClO_4 complexes were more active on the investigated cell lines, while only a moderate activity for [Pt(bpy)(Δ-Hbie)]Cl, [Pd(bpy)(Δ-Hbie)]Cl, [Ag(Δ-H_2bie)$_2$]ClO_4 and [Ag(Λ-H_2bie)$_2$]ClO_4 was noted (Scheme 2).

In general, the PPh_3 and phen complexes are more active against the tested cell lines than are their bpy-analogues. DNA is the major cellular target for the metal complexes and the greater

hydrophobicity of the ancillary ligand (PPh_3 or phen) may lead to a better cellular uptake and to a higher cytotoxicity [92]. In addition, there is also another weakly discernible trend between the cell lines in that the compounds showed higher activities against MDA-MB231 human breast cancer cells, which are oestrogen receptor (ER)-negative *vs.* breast cancer cells [93].

DNA synthesis is known to be critical to cell division. Therefore, any chemotherapeutic agent that can significantly inhibit DNA synthesis is likely to be of particular interest in controlling cancer cell division. The data presented here suggest that the presence PPh_3 or phen as a secondary ligand serves to enhance the cytotoxicity of the complexes and these are capable of inhibiting DNA synthesis in both cell lines and in a concentration-dependent manner (Fig. 8). Furthermore, at the concentrations studied (0.003125-100 μM), the pair of enantiomeric Ag(I)-PPh_3 complexes, $[Ag(PPh_3)(\Lambda\text{-}H_2bie)]ClO_4$ and $[Ag(PPh_3)(\Delta\text{-}Hbie)]$, showed much lower cytotoxic potency than did *cisplatin*. In particular, at the low concentration of 0.003125 M, the Ag-PPh_3 complexes maintained the inhibition rates of 0.85 and 0.49 % {$[Ag(PPh_3)(\Lambda\text{-}H_2bie)]ClO_4$}, 2.1 and 1.73% {$[Ag(PPh_3)(\Delta\text{-}Hbie)]$} while the rate for *cisplatin* was 6.2 and 3.96 % for the MDA-MB231 and OVCAR-8 cell lines, respectively [73].

The final IC_{50} values for cell growth proliferation of the pair of enantiomeric Ag(I)-PPh_3 complexes $[Ag(PPh_3)(\Lambda\text{-}H_2bie)]ClO_4$ and $[Ag(PPh_3)(\Delta\text{-}Hbie)]$ were 0.443 and 1.277 μM, respectively, for the human breast cancer (MDAMB231) cell line, while for human ovarian cancer (OVCAR-8) cell line, the values were 0.427 and 1.437 μM, respectively. The $[Ag(PPh_3)(\Lambda\text{-}H_2bie)]ClO_4$ enantiomer is more active than its analogue, $[Ag(PPh_3)(\Delta\text{-}Hbie)]$. This feature may be attributed to the mode of chelation, which is neutral bidentate (through –OH and N=C) in the former and mono-negative bidentate (*via* $-O^-$ and N=C) in the latter. The Ag-OH

bond is stronger than is the Ag-O one, i.e. the hydrolysis of the former is more difficult and it takes more time to reach the DNA, reflecting its activity.

An important property that Pt-N and Pd-N donors have is that the thermodynamic strengths of the typical coordination bonds are much weaker than C-C, C-N or C-S covalent bonds. Moreover, ligand exchange in Pt(II) complexes is quite slow, which gives them high kinetic stability. Thus, the ligand exchange reactions take place in minutes to days, rather than microseconds to seconds, as in case of Pd(II) complexes [32]. This feature explains the activity of [Pt(phen)(Δ-Hbie)]Cl, [Pt(phen)(Λ-Hbie)]Cl and [Pt(bpy)(Δ-Hbie)]Cl compared to their Pd(II) analogues, [Pd(phen)(Δ-Hbie)]Cl, [Pd(phen)(Λ-Hbie)]Cl and [Pd(bpy)(Δ-Hbie)]Cl [32,43].

3.6.2. Circular dichroism spectra

Circular dichroism (CD) spectroscopy is an optical technique that is used to measure the difference in the absorption of left and right circularly polarized light [94]. It is widely employed in studying nucleic acid structures as well as monitoring the conformational polymorphism of DNA [95,96]. The DNA molecule may undergo conformational changes to the B-form, A-form, Z-form, quadruplexes, triplexes and other structures as a result of the binding processes to different compounds [95]. Because DNA replication is a key event for cell division, it is a critically important target in cancer chemotherapy.

DNA is the primary pharmacological target of many antitumor compounds [97], DNA-metal complex interactions have paramount importance in understanding the mechanism of tumor inhibition in the treatment of cancer. As mentioned already, CD spectroscopy has been used to obtain structural information about the global changes in DNA conformations induced by metal complexes. However, a variety of platinum complexes act as DNA intercalators upon

coordinating the appropriate ancillary ligands [98]. The interactions of Pd(II) derivatives with DNA in both covalent [99] and non-covalent ways have been reported [100]. One particularly important field of research is based on efforts to understand the DNA binding properties of transition metal complexes in the hope of developing novel probes for nucleic acid structures, antitumor agents, DNA foot printing and sequence specific cleaving agents, etc. [101–104]. The pair of enantiomers 1,2-bis(1H-benzimidazol-2-yl)-1,2-ethanediol, Δ-H_2bie and Λ-H_2bie, ligands may be of particular interest for these applications owing to their chiral structures [55]. A study of enantioselective complex–DNA binding by CD spectroscopy may furnish direct information on how the DNA helix and the enantiomeric complexes interact and thus reveal the influence of each enantiomer of a given complex on the DNA-binding strength. The CD spectra of the pair of enantiomers, Δ-H_2bie and Λ-H_2bie, and the complexes, {[Ag(Δ-Hbie)(PPh_3)] and [Ag(Λ-H_2bie)(PPh_3)]ClO_4}, {[Pt(phen)(Δ-Hbie)]Cl and [Pt(phen)(Λ-Hbie)]Cl}, {[Pd(phen)(Δ-Hbie)]Cl and [Pd(phen)(Λ-Hbie)]Cl} as well as [Pt(Δ-Hbie)(PPh_3)Cl and [Ag(phen)(Δ-Hbie)], in 5 mM phosphate buffer - 50 mM NaCl (pH 7.2) have been measured (Figs. 9-11). The CD patterns observed for circulating tumor DNA (CT-DNA) may provide further and definitive confirmation of the probable mode of CT-DNA binding of the reported complexes, which is depicted by the perturbation induced in the DNA morphology upon the binding of complexes to CT-DNA. The two bands of CT-DNA (positive at 275 nm and negative at 245 nm due to base stacking and helicity, respectively, i.e., the right-handed B form [95,96]) are the net result of coupling interactions of the bases, which depend on the skewed orientation of the CT-DNA backbone [105]. The effect of the complexes on the conformation of the secondary structure of DNA has been studied by keeping the concentration of CT-DNA at 2.67 x 10^{-5} mM while varying the concentration of the complexes (0.5607 x 10^{-5}-3.34642 x 10^{-5} mM); [complex]/[CT-DNA] = 0,

0.21, 0.42, 0.63, 0.86, 1.05, 1.26….etc. Simple groove binding and electrostatic interaction of the complexes with DNA show less or no perturbation on the base stacking, while intercalation interactions result in the enhancement of the intensities of both bands [106].

Upon addition of the pairs of enantiomeric Δ-H_2bie and Λ-H_2bie complexes, {[Pd(phen)(Δ-Hbie)]Cl and [Pd(phen)(Λ-Hbie)]Cl}, {[Pt(phen)(Δ-Hbie)]Cl and [Pt(phen)(Λ-Hbie)]Cl} (Fig. 11) to CT-DNA, almost identical CD changes of equal magnitude, but of opposite sign, were observed in the CD spectra. This result may be due to either the different matching between the enantiomers and DNA or the different binding sites of the enantiomers because DNA is a flexible double helix and the complex can intercalate towards the DNA helix axis from any direction [107,108]. A detectable difference was observed in the interaction of both enantiomers with CT-DNA; the Δ-enantiomer binds DNA more strongly than the Λ-enantiomer *via* intercalation. Similar features have been reported for the enantiomeric {Δ-$[Ru(bpy)_2(nfip)]^{2+}$ and Λ-$[Ru(bpy)_2(nfip)]^{2+}$} and {Δ-$[Ru(bpy)_2(HPIP)](PF_6)_2$ and *Λ*-$[Ru(bpy)_2(L)](PF_6)_2$ (L = 2-(2-hydroxyphenyl)imidazo[4,5-*f*][1,10]phenan-throline), 2-(2-hydroxy-1-naphthyl)imidazo[4,5-*f*][1,10]phenanthroline), 2-(2-hydroxy-5-nitrophenyl)imidazo [4,5-*f*][1,10]phenanthroline), dipyridophenazine)} complexes [107,108]. From the CD spectral data, we can essentially discriminate the enantio-preferential binding of DNA between Δ-H_2bie and Λ-H_2bie complexes [109].

Upon the addition of the Λ-H_2bie enantiomers, [Pd(phen)(Λ-Hbie)]Cl or [Pt(phen)(Λ-Hbie)]Cl, to CT-DNA (Fig. 10), there are changes in both the positive and negative bands, including a decrease in the intensities of the negative bands. The decrease in ellipticity is due to destabilization of the DNA form and is attributed to opening of the DNA structure by the formation of intrastrand DNA cross-linking [106,110]. The decrease in the intensity of the

positive band suggests that the complex can unwind the DNA helix and lead to a loss of helicity [106,111]. Moreover, the multifaceted binding mode observed for the enantiomers [Pd(phen)(Λ-Hbie)]Cl or [Pt(phen)(Λ-Hbie)]Cl promotes their strong binding to DNA, so that there is effective screening of the negative charge on the N7 base site and the phosphate oxygen atom simultaneously along the phosphate backbone. This feature supports a *trans*-conformational change of the DNA double helical conformation [112]; the electrostatic components of the interactions are effective in bringing about such *trans*-conformational changes. Further transformation of the DNA structure proceeds by removal of labile groups attached in the complexes, which results in removal of water from the base sites and grooves in the DNA helix, leading to an effective binding of the complex to DNA [109]. The CD spectrum of DNA shows a significant decrease in intensity of the positive band upon addition of the enantiomers, [Pd(phen)(Λ-Hbie)]Cl and [Pt(phen)(Λ-Hbie)]Cl, which reveals a right-handed conformational change of the DNA double helix, possibly due to its partial intercalative binding of the complexes.

When the B-DNA to A-DNA transition occurs, the CD band at 245 nm shifts toward higher wavelength and the band at 275 nm becomes more intense [96]. The binding of [Ag(Δ-Hbie)(PPh_3)], [Pt(Δ-Hbie)(PPh_3)Cl and [Ag(phen)(Δ-Hbie)] with CT-DNA causes a shift in these marker CD bands, indicating an alteration in B-DNA conformation. This situation is further confirmed by the IR spectra of the [Ag(phen)(Δ-Hbie)]-DNA and [Pt(phen)(Δ-Hbie)]Cl-DNA interactions, which show shifts of the 1228 (PO_2) and 836 (phosphodiester) bands to ~1240 and 815 cm^{-1}, respectively [97]. Furthermore, upon increasing the concentration of the complexes, the CT-DNA spectra show a remarkable increase in the positive band ellipticity together with a red shift [113,114], which may be due to phen or PPh_3 $\pi \rightarrow \pi^*$ transitions. These electronic

transitions are quite sensitive to the increased positive base pair tilting of A-DNA [113]. This observation supports the intercalative binding for the complexes. Insertion of the complex into adjacent base pairs prevents neighboring base pairs from close stacking, leading to an enhancement in the positive CD band [114,115].

Conclusions

The preparation and structural characterization of new Pd(II), Pt(II) and Ag(I) complexes based on (Δ)- and (Λ)-1,2–bis-(1H-benzimidazol-2-yl)-1,2-ethanediol (Δ-H_2bie and Λ-H_2bie) enantiomers in the absence and presence of the N,N-chelating ligands (2,2'-bipyridyl, 9,10-phenanthroline) and triphenylphosphine have been described. The *in vitro* anticancer activity of the complexes against human breast (MDA-MB231) and ovarian (OVCAR-8) cancer cell lines has been evaluated. Δ-H_2bie complexes proved to be more active against the studied cell lines. The order for cytotoxic activities of the complexes is Ag(I)-PPh_3 > Ag(I)-phen > Pt(II)-phen > Pd(II)-phen > Ag(I)-bpy > Ag(I) > Pt(II)-bpy > Pd(II)-bpy > Pt(II)-PPh_3 > Pd(II)-PPh_3 > Pd(II) > Pt(II). The CT-DNA-binding properties of some of the complexes have been studied by CD spectroscopy. The intercalation interactions of the Δ-enantiomers are stronger than those of the Λ- enantiomers. All the complexes have intercalative CT-DNA binding capabilities.

Acknowledgements

We are grateful to the Ministry of Higher Education in Egypt (A. A. Shabana) and a NSERC (Canada) Discovery grant (I.S.B.) for financial support of this work.

References

[1] H. A. Barker, R. D. Smyth, H. Weissbach, J. I. Toohey, J. N. Ladd, B. E. Volcani, J. Biol. Chem., 235, 1960, 480-288.

[2] N. S. Pawar, D. S. Dalal, S. R. Shimpi, P. P. Mahulikar, Eur. J. Pharm. Sci., 21, 2004, 115-118; İ. Ören, Ö. Temiz, İ. Yalçin, E. Şener, N. Altanlar, Eur. J. Pharm. Sci., 7, 1998, 153-160.

[3] T. Hisano, M. Ichikawa, K. Tsumoto, M. Tasaki, Chem. Pharm. Bull., 30, 1982, 2996-3004; K. K. Mothilal, C. Karunakaran, A. Rajendran, R. Murugesan, J. Inorg. Biochem., 98, 2004, 322-332.

[4] S. Özden, D. Atabey, S. Yildiz, H. Göker, Bioorg. Med. Chem., 13, 2005, 1587-1497; Y. He, B. Wu, J. Yang, D. Robinson, L. Risen, R. Ranken, L. Blyn, S. Sheng, E. E. Swayze, Bioorg. Med. Chem. Lett., 13, 2003, 3253-3256.

[5] T. C. Kühler, M. Swanson, B. Christenson, A. C. Klintenberg, B. Lamm, J. Fägherhag, R. Gatti, M. Ölwegård-Halvarsson, V. Shcherbuchin, T. Elebring, J. Sjöström, J. Med. Chem., 45, 2002, 4282-4299.

[6] D. Carcanague, Y. Shue, M. Wuonola, M. Uria-Nickelsen, C. Joubran, J. K. Abedi, J. Jones, T. C. Kühler, J. Med. Chem., 45, 2002, 4300-4309.

[7] S. Liu, W. Cao, L. Yu, W. Zheng, L. Li, C. Fan, T. Chen, Dalton Trans., 42, 2013, 5932-5940.

[8] F. J. Yoe-Reyes, S. Bernes, N. Barba-Behrens, Acta Crystallogr., 61, 2005, 875-876; E. Şahin, S.Ide, M. Kurt, S. Z. Yurdakul, Kristallogr., 218, 2003, 385-387.

[9] M. Bukowska-Strzyzewska, A. Tosik, J. Crystallogr. Spectrosc. Res., 21, 1991, 379; A. Tosik, M. Bukowska-Strzyzewska, J. Chem. Cryst., 24, 1994, 139; A. Tosik, W.

Maniukiewicz, M. Bukowska-Strzyzewska, J. Mrozinski, M. P. Sigalas, C. A. Tsipis, Inorg. Chim. Acta, 190, 1991, 193-203.

[10] A. Tosik, M. Bukowska-Strzyzewska, J. Mrozinski, J. Coord. Chem., 24 1991, 113-120; Y. Q. Zhang, D. J. Xu, J. R. Su, Acta Crystallogr., 59, 2003, 919-920; M. E. Cruz-Núñez, B.Sc. Thesis, Universidad Nacional Autónoma de México, 2007.

[11] D. D. Lin, Y. Liu, D. J. Xu, Acta Crystallogr., 59, 2003, 771; Y. H. Xue, D. D. Lin, D. J. Xu, Acta Crystallogr., 59, 2003, 750-752; A. Tosik, L. Sieron, M. Bukowska-Strzyzewska, Acta Crystallogr., Sect. C: Cryst. Struct. Commun., 51, 1995, 1987-1988.

[12] A. Ceniceros-Gómez, N. Barba-Behrens, M. E. Quiroz-Castro, S. Bernes, H. Nöth, S. E. Castillo-Blum, Polyhedron, 19, 2000, 1821-1827.

[13] C. Bolm, N. Meyer, G. Raabe, T. Weyermüller, E. Bothe, Chem. Commun., 2000, 2435-2436.

[14] G. A. v. Albada, J. Reedijk, R. Hämäläinen, U. Turpeinen, A. L. Spek, Inorg. Chim. Acta, 163, 1989, 213-222.

[15] E. Z. Jahromi, A. Divsalar, A. A. Saboury, S. Khaleghizadeh, H. Mansouri□Torshizi, I. Kostova, J. Iran. Chem. Soc., 13, 2016, 967–989; P. Christakis, J. Biol. Med., 84, 2011, 169-172.

[16] R.S. Kumar, S. Arunachalam, V.S. Periasamy, C.P. Preethy, A. Riyasdeen, M.A. Akbarsha, J. Inorg. Biochem., 103, 2009, 117-127.

[17] C. Deegan, M. McCann, M. Devereux, B. Coyle, D.A. Egan, Cancer Lett., 247, 2007, 224-233.

[18] A.M. Florea, D. Büsselberg, Cancers, 3, 2011, 1351-1371.

[19] R. Silavi, A. Divsalar, A.A. Saboury, J. Biomol. Struct. Dyn., 30, 2012, 752-772.

[20] A. Divsalar, A.A. Saboury, R. Yousefia, A.A. Moosavi-Movahedi, H. Mansoori-Torshizi, Int. J. Biol. Macromol., 40, 2007, 381-386.

[21] A. Divsalar, A.A. Saboury, H. Mansoori-Torshizi, M.I. Moghaddam, F. Ahmad, G.H. Hakimelahi, J. Biomol. Struct. Dyn., 26, 2009, 587-597.

[22] A. Divsalar, A.A. Saboury, L. Ahadi, E. Zemanatiyar, H. Mansouri-Torshizi, D. Ajloo, R.H. Sarma, J. Biomol. Struct. Dyn., 29, 2011, 283-296.

[23] I. Kostova, Pat. Anti-Cancer Drug Discov., 1, 2006, 1-22.

[24] R.T. Dorr, A review of the modulation of cisplatin toxicities by chemoprotectants, in Platinum and Other Metal Coordination Compounds in Cancer Chemotherapy, 2nd edn., ed. by H.M. Pinedo, J.H. Schornagel (Plenum Press, New York, 1996), p. 131; H. Mansoori-Torshizi, M.I. Moghaddam, A. Divsalar, A.A. Saboury, J. Biomol. Struct. Dyn., 26, 2009, 575-586.

[25] L. Yan, X. Wang, Y. Wang, Y. Zhang, Y. Li, Z. Guo, J. Inorg. Biochem., 2012, 106, 46.

[26] A.C. Moro, A.E. Mauro, A.V.G. Netto, S.R.A. Nanias, M. B. Quilles, I.Z. Carlos, F.R. Pavan, C.Q.F. Leite, M. Horner, Eur. J. Med. Chem., 44, 2009, 4611-4615.

[27] I. Brudzinska, Y. Mikata, M. Obata, C. Ohtsuki, S. Yanoa, Med. Chem. Lett., 14, 2004, 2533-2536.

[28] C.A. Rabik, M.E. Dolan, Cancer Treat. Rev., 33, 2007, 9-23.

[29] A.M. Montana, F.J. Bernal, J. Lorenzo, C. Farn´os, C. Batalla, M.J. Prieto, V. Moreno, F.X. Avil´es, J.M. Mesas, M.T. Alegre, Bioorg. Med. Chem., 16, 2008, 1721-1728.

[30] L.R. Kelland, S.Y. Sharp, C.F.O. O'Neill, F.I. Raynaud, P.J. Beale, I.R. Judson, J. Inorg. Biochem., 77, 1999, 111-115.

[31] S. Ahmad, Chem. Biodiv., 7, 2010, 543–566.

[32] S. Nadeem, M. Bolte, S. Ahmad, T. Fazeelat, S.A. Tirmizi, M.K. Rauf, S.A. Sattar, S. Siddiq, A. Hameed, S.Z. Haider, Inorg. Chim. Acta, 363, 2010, 3261-3269.

[33] I.H. Krakoff, In Platinum and Other Metal Coordination Compounds in Cancer Chemotherapy, ed. by M. Nicoline (Springer, US, 1988), p. 351

[34] E.R. Jamieson, S.J. Lippard, Chem. Rev., 99, 1999, 2467-2498.

[35] E. Wong, C.M. Giandomenico, Chem. Rev., 99, 1999 , 2451-2461.

[36] M.L. Chen, C.H. Fang, L.S. Liang, L.H. Dai, X.K. Wang, Surg. Oncol., 19, 2010, 38-45.

[37] N.J. Wheate, J.G. Collins, Coord. Chem. Rev., 241, 2003, 133-145.

[38] S. Carotti, G. Marcon, M. Marussich, T. Mazzei, L. Messori, E. Mini, P. Orioli, Chem. Biol. Interact., 125, 2000, 29-37.

[39] F. Dallavalle, F. Gaccioli, R. Franchi-Gazzola, M. Lanfranchi, L. Marchio, M.A. Pellinghelli, M.J. Tegoni, J. Inorg. Biochem., 92, 2002, 95-104.

[40] A. Divsalar, A.A. Saboury, H. Mansouri-Torshizi, B. Hemmatnejad, Bull. Korean Chem. Soc., 27, 2006, 1801-1808.

[41] M. Saeidfar, H. Masouri-Torshizi, G.R. Behbehani, A. Divsalar, A.A. Saboury, Bull. Korean Chem. Soc., 30, 2009, 1951-1955

[42] G. Rezaei Behbehani, A. Divsalar, A.A. Saboury, M.J. Bagheri, J. Sol. Chem., 37, 2008, 1785-1794.

[43] J.L. Butour, S. Wimmer, F. Wimme, P. Castan, Chem. Biol. Interact., 104, 1997, 165-178.

[44] J. Kuduk-Jaworska, A. Puszko, M. Kubiak, M. Pełczynska, J. Inorg. Biochem., 98, 2004, 1447-1456; M. Juribašić, K. Molcˇanov, B. Kojić-Prodić, L. Bellotto, M. Kralj, F. Zani, L. Tušek-Božić, J. Inorg. Biochem., 105, 2011, 867-879.

[45] J. M. Vujic, M. Cvijovic, G.N. Kaluderovic, M. Milovanovic, B.B. Zmejkovskic, V. Volarevic, N. Arsenijevic, T.R. Sabo, S.R. Trifunovic, Eur. J. Med. Chem., 45, 2010, 3601-3606.

[46] G. Faraglia, D. Fregona, S. Sitran, L. Giovagnini, C. Marzano, F. Baccichetti, U. Casellato, R. Graziani, J. Inorg. Biochem., 83, 2001, 31-43.

[47] L. Giovagnini, L. Ronconi, D. Aldinucci, D. Lorenzon, S. Sitran, D. Fregona, J. Med. Chem., 48, 2005, 1588-1595.

[48] W. P. Griffith, S. I. Mostafa, Polyhedron, 11, 1992, 2997-3005.

[49] P. Skehan, R. Storeng, D. Scudiero, J. Natl. Cancer Inst., 82, 1990, 1107-1112.

[50] J. Murmur, J. Mol. Biol., 3, 1961, 208; N. Raman, K. Pothiraj, T. Baskaran, J. Mol. Struct., 1000, 2011, 135-144.

[51] W. Geary, Coord. Chem. Rev., 7, 1971, 81.

[52] E. E. S. Teotonio, J. G.P. Espı´nola, H. F. Brito, O. L. Malta, S. F. Oliveira, D. L.A. de Faria, C. M. S. Izumi, Polyhedron 21, 2002, 1837-1846.

[53] K. Isele, V. Broughton, C. J. Matthews, A. F. Williams, G. Bernardinelli, P. Franz, S. Decurtins J. Chem. Soc., Dalton Trans., 2002, 3899-3905.

[54] A. Tavman, J. Serb. Chem. Soc., 71, 2006, 521-528.

[55] S. Parveen, F. Arjmand, Spectrochim. Acta A, 85, 2012, 53-60.

[56] M. Chauhan, F. Arjmand, Chem. Biodivers., 3, 2006, 660-675.

[57] G. F. de Sousa, V. M. Deflon, M. T. P. Gambardella, R. H. P. Francisco, J. D. Ardisson, E. Niquet, Inorg. Chem., 45, 2006, 4518-4525.

[58] A. Tavman, Rev. Inorg. Chem., 22, 2002, 113-119.

[59] A. Tavman, C. Sayil, J. Serb. Chem. Soc., 80(1), 2015, 45; A. Tavman, Main Group Met.

Chem., 26, 2003, 229-235.

[60] H. Li, J. Li, H. Chen, Y. Zhang, D. Huang, J. Chem. Crystallogr., 41, 2011, 1844-1846.

[61] S. Mostafa, C. Papatriantafyllopoulou, S. Perlepes, N. Hadjiliadis, Bioinorg. Chem. Appl., 2008, doi:10.1155/2008/647873; A. G. de A. Fernandes, V. M. Deflon, E. J. de Souza, P. I. S. Maia, A. A. Batista, S. S. Lemos, U. Abram, J. Ellena, E. E. Castellano, Polyhedron, 27, 2008, 2983-2989.

[62] A. Ouf, M. S. Ali, E. M. Saad, S. I. Mostafa, J. Mol. Struct., 973, 2010, 69-75.

[63] I. Gabr, H. El-Asmy, M. Emmam, S. I. Mostafa, Transition Met. Chem., 34, 2009, 409-418.

[64] Y. Li, C. Jan, Y. Zheng, D. Liao, Polyhedron, 17, 1998, 1423-1428; S. A. El Sayed, A. M. El Hendawy, S. I. Mostafa, I. S. Butler, Inorg. Chim. Acta, 363, 2010, 2526-2532.

[65] S. Mostafa, A. El-Asmy, M. El-Shahawi, Transition Met. Chem., 25, 2000, 470-473.

[66] K. Nakamoto, Wiley, New York, 1986.

[67] F. A. Bovey, SN.M.R. Data for Organic Compounds T, Interscience, 1967.

[68] F. A. El-Morsy, B. J. Jean-Claude, I. S. Butler, S. A. El-Sayed, S. I. Mostafa, Inorg. Chim. Acta, 423, 2014, 144-155.

[69] S. I. Mostafa, Transition Met. Chem., 24, 1999, 306-310.

[70] S. A. Elsayed, A.M. El-Hendawy, I.S. Butler, S.I. Mostafa, J. Mol. Struct., 1036, 2013, 196-202; S. I. Mostafa, Transition Met. Chem., 23, 1998, 397-401.

[71] I. S. Butler, D. F. R. Gilson, B. J. Jean-Claude, S. I. Mostafa, Inorg. Chim. Acta, 423, 2014, 132-143.

[72] H. A. El-Asmy, I. S. Butler, Z. S. Mouhri, B. J. Jean-Claude, M. S. Emmam, S. I. Mostafa, J. Mol. Struct., 1059, 2014, 193-201.

[73] S. A. ElSayed, I. S. Butler, B. J. Jean-Claude, S. I. Mostafa, Transition Met. Chem., 40,

2015, 179-187.

[74] E. L. Muetterties, C. W. Alegranti, J. Am. Chem. Soc., 94, 1972, 6386-6391.

[75] D. C. Onwudiwe and P. A. Ajibade, Int J. Mol. Sci., 13(8), 2012, 9502-9513; A. K. Jassal, S. Sharma, G. Hundal, and M. S. Hundal, Cryst. Growth Des., 15(1), 2015, 79-93.

[76] A. A. Shabana, I. S. Butler, D. F.R. Gilson, B. J. Jean-Claude, Z. S. Mouhri, M. M. Mostafa, S. I. Mostafa, Inorg. Chim. Acta, 423, 2014, 242-255.

[77] S. A. Elsayed, B. J. Jean-Claude, I. S. Butler, S. I. Mostafa, J. Mol. Struct., 1028, 2012, 208-214.

[78] S. I. Mostafa, F. A. Badria, Metal-Based Drugs, 2008, doi: 10.1155/2008/723634.

[79] S. I. Mostafa, S. P. Perlepes, N. Hadjiliadis, Z. Naturforsch., 56b, 2001, 394-402.

[80] Sh. A. Kadirova, M. R. Tursunova, M. M. Ishankhodzhaeva, N. A. Parpiev, Z. Karimov, A. Tozhiboev, B. Tashkhodzhaev, Russ. J. General Chem., 77, 2007, 1807-1816.

[81] T. D. Thangadurai, K. Natarajan, Transition Met. Chem., 26, 2001, 717-722.

[82] S. I. Mostafa, S. Abd El-Maksoud, Monatsh. Chem., 129, 1998, 455-466.

[83] I. C. Mendes, L. M. Botion, A. V. M. Ferreira, E. E. Castellano, H. Beraldo, Inorg. Chim. Acta, 362, 2009, 414-420; T. S. Lobana, G. Bawa, R. J. Butcher, C. W. Liu, Anorg. Z. Allg. Chem., 635, 2009, 355-360.

[84] I. Agranat, H. Caner, J. Caldwell, Nat. Rev. Drug Discov., 1, 2002, 753-768.

[85] J. K. Barton, Science, 233, 1986, 727–734.

[86] K. H. Thompson, C. Orvig, Science, 300, 2003, 936; J. Reedijk, Proc. Natl. Acad. Sci. U.S.A., 7, 2003, 3611-3616.

[87] T. Storr, K. H. Thomposon, C. Orvig, Chem. Soc. Rev., 35, 2006, 534-544.

[88] S. C. Stinson, Chem. Eng. News, 79, 2001, 45; Q. Xiaogang, J. O. Trent, I. Fokt, W.

Priebe, J. B. Chaires, Proc. Natl. Acad. Sci. U.S.A., 97, 2000, 12032-12037.

[89] M. Gökçe, S. Utku, S. Gür, A. Ozkul, F. Gümüş, Eur. J. Med. Chem., 40, 2005, 135-141.

[90] K. Vickery, A. M. Bonin, R. R. Fenton, S. O'Mara, P. J. Russell, L. K. Webster, T. W. Hambley, J. Med. Chem., 36, 1993, 3663.

[91] M. Carreira, R. Calvo-Sanjuan, M. Sanau, X. Zhao, R. S. Magliozzo, I. Marzo, M. Contel, J. Inorg. Biochem., 116, 2012, 204-214.

[92] F. A. Beckford, M. Shaloski, Jr., G. Leblanc, J. Thessing, L. C. Lewis-Alleyne, A. A. Holder, L. Li, N. P. Seeram, Dalton Trans., 2009, 10757-10764.

[93] H. Harrison, B. M Simões, L. Rogerson, S. J Howell, G. Landberg, R. B Clarke, Breast Cancer Research, 15, 2013, R21; M. J. Scandlyn, E. C. Stuart, T. J. Somers-Edgar, A. R. Menzies, R. J. Rosengren, British J. Cancer, 99, 2008, 1056-1063.

[94] 1. Woody, R.W. Circular dichroism. Meth. Enzymology, 246, 1995, 34-71.

[95] N. Shahabadi, S. Mohammadi, R. Alizadeh, Bioinorg. Chem. Appl., 2011, 1-8, doi:10.1155/2011/429241.

[96] F. Arjmand, B. Mohani, S. Parveen, Bioinorg. Chem. Appl., 2006, 1, doi. 10.1155/BCA/2006/32896.

[97] C. N. N,soukpoe-Kossi, A. Ahmed Ouameur, T. Thomas, A. Shirahata, T. J. Thomas,H. A. Tajmir Riahi, Biomacromolecules, 9, 2008, 2712-2718.

[98] H. K. Liu, P. J. Sadler, Acc. Chem. Res., 44, 2011, 349-359.

[99] E. Gao, M. Zhu, L. Liu, Y. Huang, L. Wang, C. Shi, Z. Chuyue, W. Sun, Inorg. Chem., 49, 2010, 3261–3270; J. Ruíz, N. Cutillas, C. Vicente, M.D. Villa, G. López, J. Lorenzo, F.X. Avilés, V. Moreno, D. Bautista, Inorg. Chem., 44, 2005, 7365-7376.

[100] H. Mansouri-Torshizi, M. I-Moghaddam, A. Divsalar, A.-A. Saboury, Bioorg. Med.

Chem., 16, 2008, 9616-6925.

[101] M. Demeunynck, C. Bailly, W.D. Wilson (Eds.), DNA and RNA Binders: From Small Molecules to Drugs, Wiley-VCH, Weinheim, 2003.

[102] M. Gielen, E.R.T. Tiekink (Eds.), Metallotherapeutic Drugs and Metal-Based Diagnostic Agents: The Use of Metals in Medicine, John Wiley & Sons, 2005.

[103] R.W.Y. Sun, D.L. Ma, E.L.M. Wong, C.M. Che, Dalton Trans., 2007, 4884-4892.

[104] C. Moucheron, New J. Chem., 33, 2009, 235-245.

[105] A. Rodger, B. Nordén, Oxford Chemistry Press, UK, 1997.

[106] A. M. Pyle, J. P. Rehmann, R. Meshoyrer, C. V. Kumar, N. J. Turro, J. K. Barton, J. Am. Chem. Soc., 111, 1989, 3051-3058.

[107] B. Sun, Y. Wang, C. Qian, J. Chu, S. Liang, H. Chao, L. Ji, J. Mol. Struct., 963, 2010, 153-159.

[108] J. Lui, B. Ye, Q. Zhang, X. Zou, Q. Zhen, X. Tian, L. Ji, J. Biol. Inorg. Chem., 5, 2000, 119-128.

[109] F. Arjiman, A. Jamsheera, J. Organomet. Chem., 696, 2011, 3572-3579.

[110] M.-V.J. de, J. Lorenzo, A.M. Montana, V. Morenzo, F.X. Aviles, J. Inorg. Biochem., 102, 2008, 973-987.

[111] K. Karidi, A. Garoufis, N. Hadjiliadis, J. Reedijk, Dalton Trans., 2005, 728-734.

[112] S. Mahadevan, M. Palaniandavar, Inorg. Chim. Acta, 254, 1997, 2910302.

[113] B. Jing, J. Dong, J. Li, T. Xu, L. Li, J. Coord. Chem., 66, 2013, 520-529.

[114] S. Ramakrishnan, M. Palaniandavar, J. Chem. Sci., 117, 2005, 179-186.

[115] S. Zhang, Y. Zhu, C. Tu, H. Wei, Z. Yang, L. Lin, J. Ding, J. Zhang, Z. Guo, J. Inorg. Biochem., 98, 2004, 2099-2106.

Figures Captions

Scheme 1: Structure of 1,2-bis(1*H*-benzimidazol-2-yl)-1,2-ethanediol (SS-1, SS-2 and R-3).

Fig. 1: Structures of (Δ)- and (Λ)-1,2–bis-(1H-benzimidazol-2-yl)-1,2-ethanediol (Δ-H_2bie and Λ-H_2bie)

Fig. 2: Structure of [Pt(phen)(Δ-Hbie)]Cl

Fig. 3: Structures of *cis*-[Pd(Λ-H_2bie)$_2$]Cl_2 **(a)** and *trans*-[Pd(Δ-H_2bie)$_2$]Cl_2 **(b)**

Fig. 4: ^{1}H NMR spectrum of Δ-H_2bie **(a)**, gCOSY (^{1}H) NMR spectrum of Λ-H_2bie **(b)** and gCOSY(H) NMR spectrum of [Pt(bpy)(Δ-Hbie)]Cl

Fig. 5: g HSQC(^{1}H-^{13}C) NMR spectrum of *cis*-[Pd(Λ-H_2bie)$_2$]Cl_2

Fig. 6: Mass spectra of [Pd(Λ-H_2bie)$_2$]Cl_2, [Pt(phen)(Λ-Hbie)]Cl and [Ag(PPh_3)(Δ-Hbie)]

Fig. 7: TGA thermograms of [Pd(Λ-H_2bie)$_2$]Cl_2**(a)**, [Pd(bpy)(Δ-Hbie)]Cl.H_2O **(b)**, [Ag(Δ-H_2bie)$_2$]ClO_4 **(c)** and [Ag(PPh_3)(Λ-H_2bie)]ClO_4 **(d)**.

Fig. 8: IC_{50} values of the (Δ-H_2bie) and (Λ-H_2bie) complexes tested against the human breast cancer (MDA-MB231) and ovarian cancer (OVCAR-8) cell lines

Scheme 2: IC_{50} values of the (Δ-H_2bie) and (Λ-H_2bie) complexes tested against the human breast cancer (MDA-MB231) and ovarian cancer (OVCAR-8) cell lines.

Fig.9: CD spectra of [Pt(Δ-Hbie)(PPh_3)Cl in H_2O and [Ag(Δ-Hbie)(phen)] in H_2O-DMSO

Fig. 10: CD spectra of [Pt(phen)(Λ-Hbie)]Cl and [Pd(phen)(Λ-Hbie)]Cl in H_2O

Fig. 11: CD spectra of {[Pd(phen)(Δ-Hbie)]Cl and [Pd(phen)(Λ-Hbie)]Cl} and {[Pt(phen)(Δ-Hbie)]Cl and [Pt(phen)(Λ-Hbie)]Cl} in H_2O

Tables Captions:

Table 2: ^{1}H NMR spectral data of Δ-H_2bie and Λ-H_2bie, and their complexes in DMSO-d_6

Table 2: ^{13}C NMR spectral data of Δ-H_2bie and Λ-H_2bie, and their complexes in DMSO-d_6

Table 3: Anticancer activity of Δ-H_2bie and its complexes against the human breast cancer (MDA-MB231) and ovarian cancer (OVCAR-8) cell lines

Table 4: Anticancer activity of Λ-H_2bie and its complexes against the human breast cancer (MDA-MB231) and ovarian cancer (OVCAR-8) cell lines

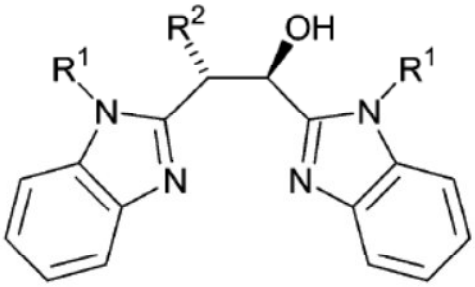

	R^1	R^2
SS-**1**	H	OH
SS-**2**	CH_3	OH
R-**3**	H	H

Scheme 1: Structure of 1,2-bis(1*H*-benzimidazol-2-yl)-1,2-ethanediol (SS-1, SS-2 and R-3).

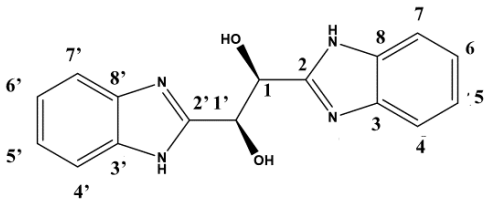

Δ-H_2bie

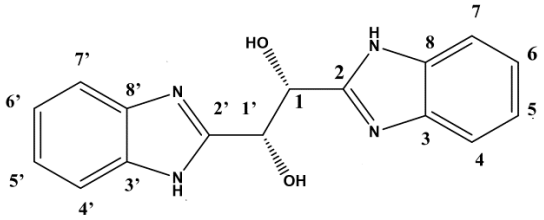

Λ-H_2bie

Fig. 1: Structure of (Δ)- and (Λ)-1,2–Bis-(1H-benzimidazol-2-yl)-1,2-ethanediol (Δ-H_2bie & Λ-H_2bie)

Fig. 2: Structure of [Pt(phen)(Δ-Hbie)]Cl

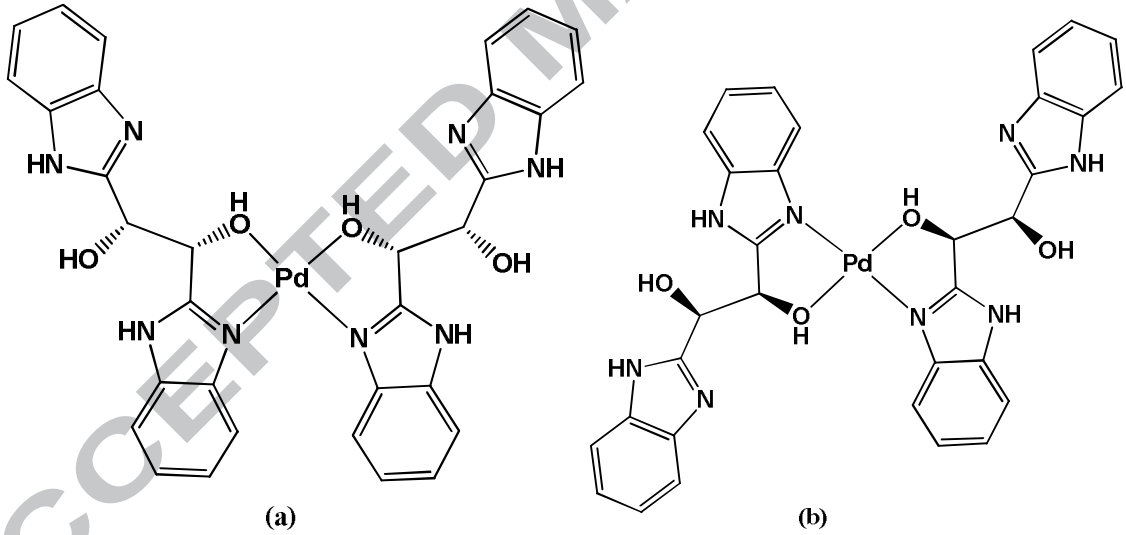

Fig. 3: Structure of *cis*-[Pd(Λ-H_2bie)$_2$]Cl_2 **(a)** and *trans*-[Pd(Δ-H_2bie)$_2$]Cl_2 **(b)**

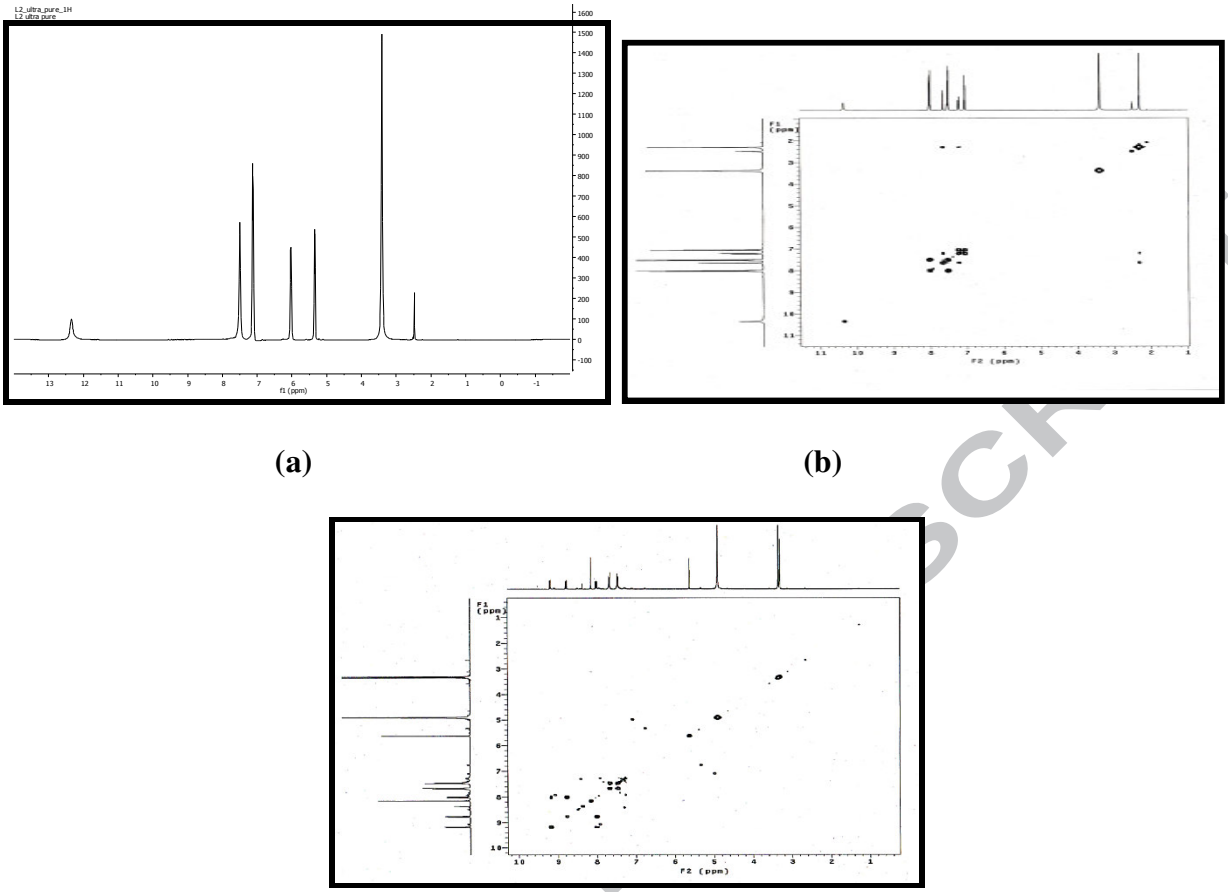

(a) **(b)**

(c)

Fig. 4: ^{1}H-NMR of Δ-H_2bie (**a**), gCOSY (^{1}H)-NMR of Λ-H_2bie **(b)** and gCOSY(H)-NMR of [Pt(bpy)(Δ-Hbie)]Cl spectra

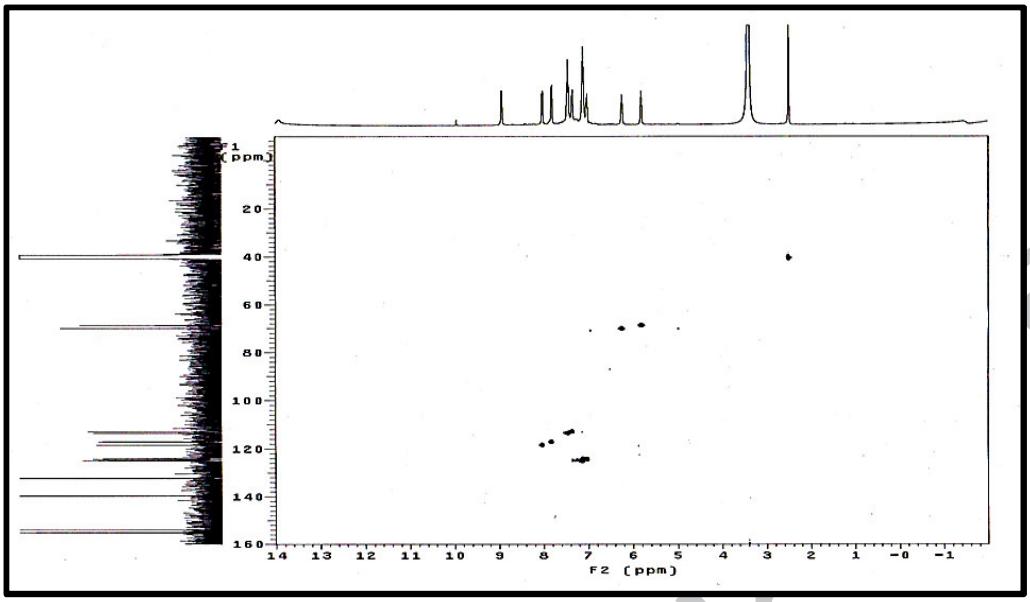

Fig. 5: g HSQC(^{1}H-^{13}C)-NMR spectrum of *cis*-[Pd(Λ-H_2bie)$_2$]Cl_2

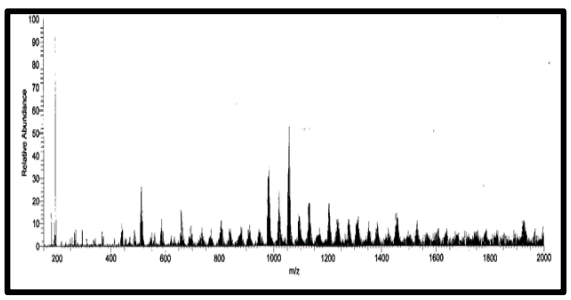

(a)

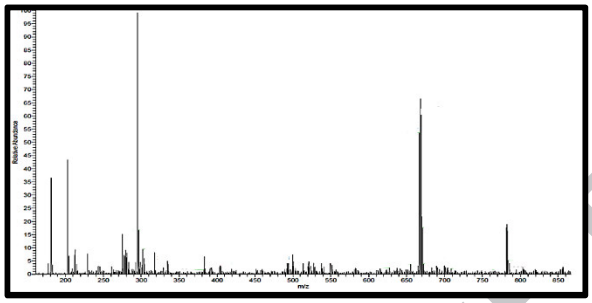

(b)

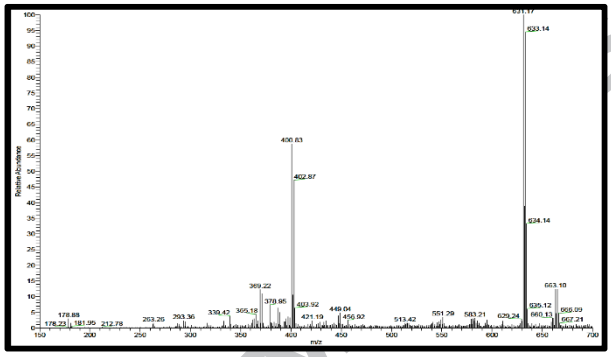

(c)

Fig. 6: Mass spectra of $[Pd(\Lambda\text{-}H_2bie)_2]Cl_2$, [Pt(phen)(Λ-Hbie)]Cl, $[Ag(PPh_3)(\Delta\text{-Hbie})]$

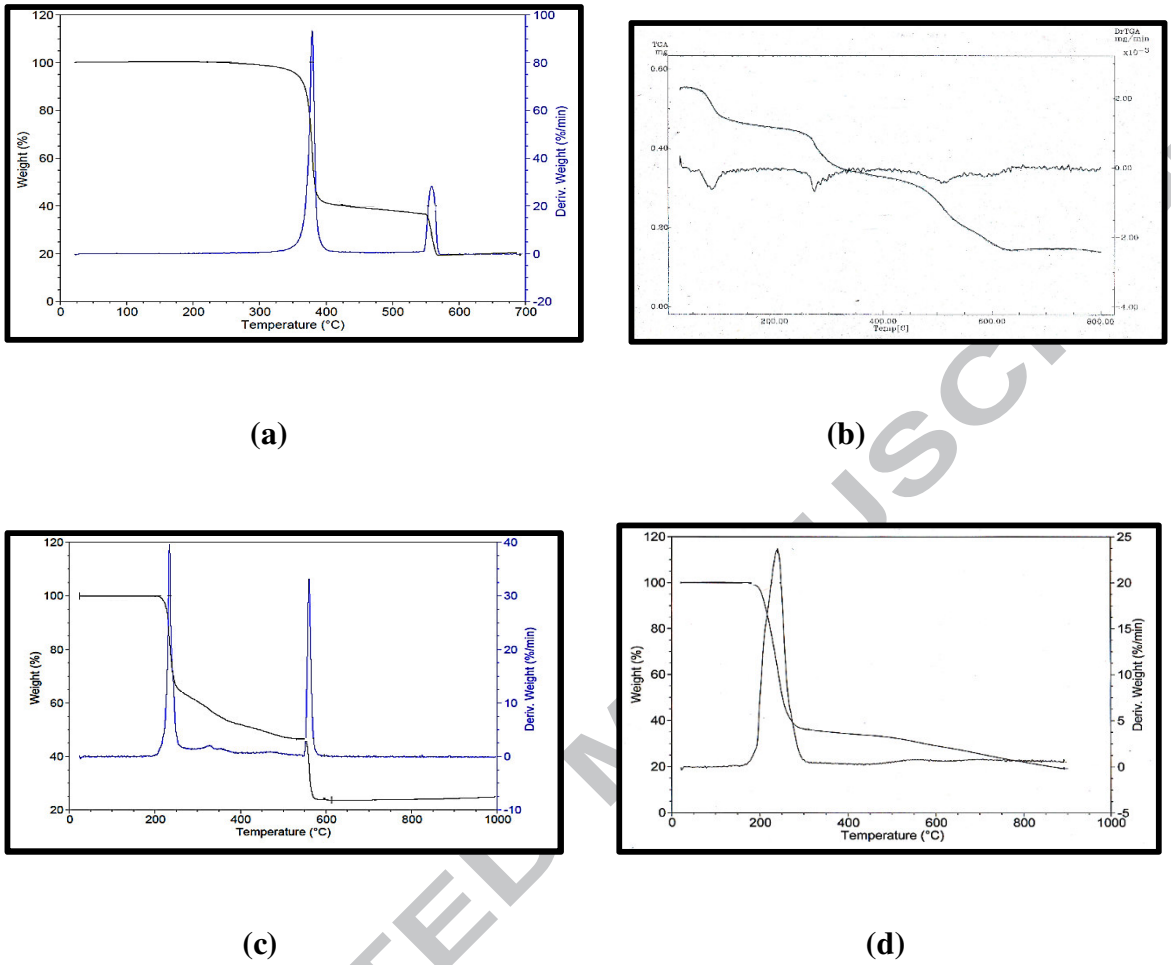

Fig. 7: TGA thermograms of $[Pd(\Lambda\text{-}H_2bie)_2]Cl_2$**(a)**, $[Pd(bpy)(\Delta\text{-}Hbie)]Cl.H_2O$ **(b),** $[Ag(\Delta\text{-}H_2bie)_2]ClO_4$ **(c),** $[Ag(PPh_3)(\Lambda\text{-}H_2bie)]ClO_4$ **(d).**

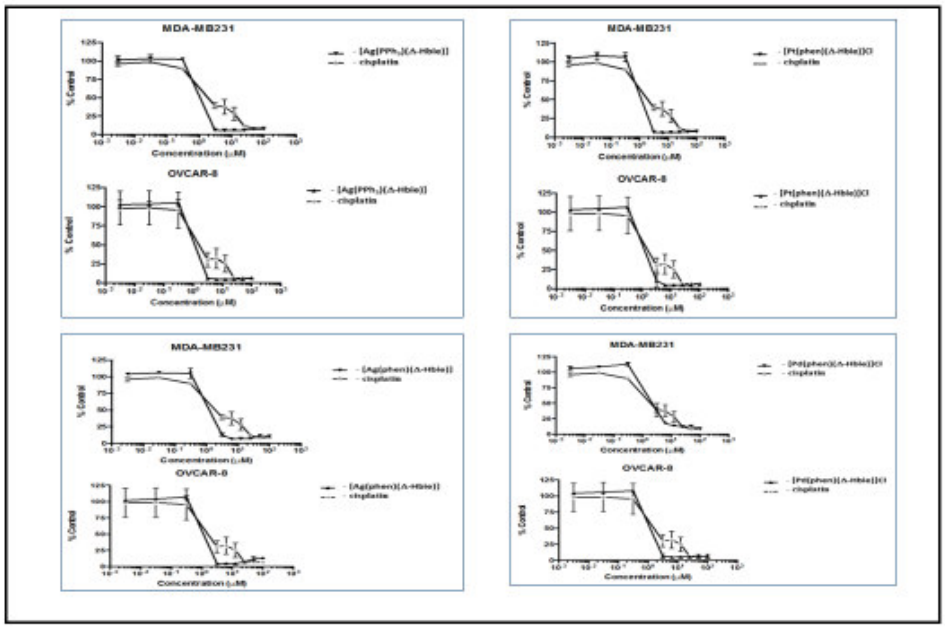

(a) [Ag(PPh$_3$)(Δ-Hbie)], [Pt(phen)(Δ-Hbie)]Cl, [Ag(phen)(Δ-Hbie)], and

(b) [Pd(phen)(Δ-Hbie)]Cl

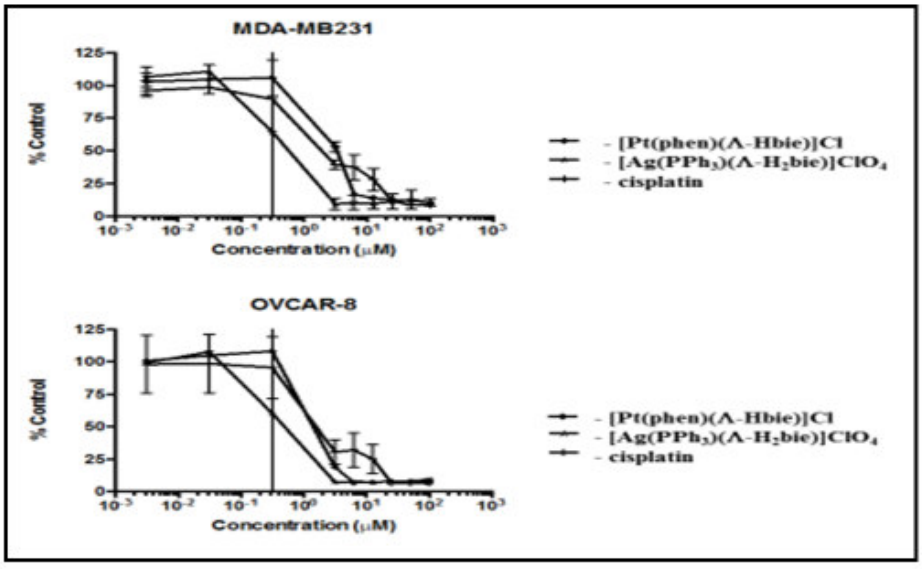

(b) [Ag(PPh$_3$)(Λ-H$_2$bie)]ClO$_4$ and [Pt(phen)(Λ-Hbie)]Cl

Fig. 8: IC_{50} values of (Δ-H_2bie) and (Λ-H_2bie) complexes, tested against the human breast cancer (MDA-MB231) and ovarian cancer (OVCAR-8) cell lines

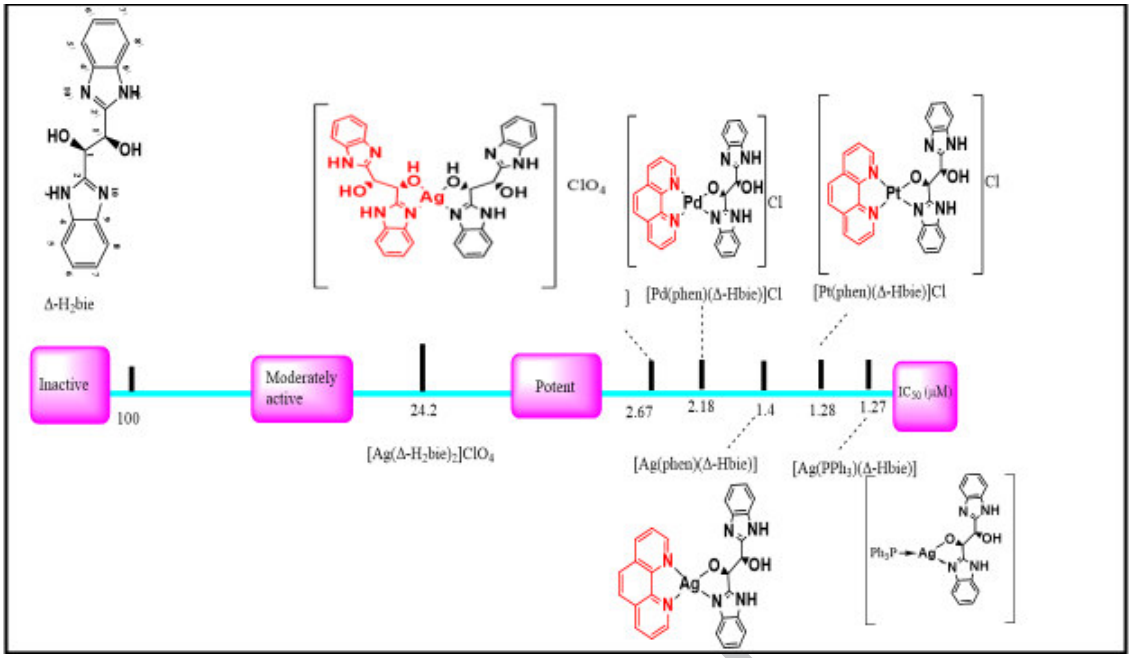

(a) Δ-H_2bie complexes

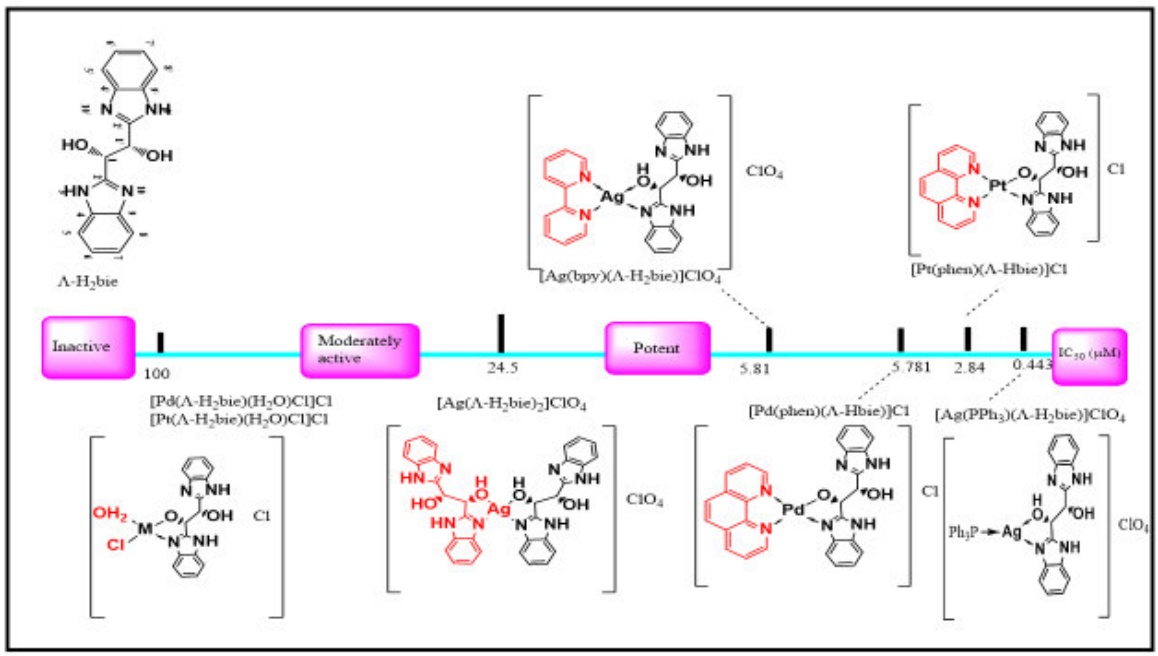

(b) Λ-H_2bie complexes

Scheme 2: IC_{50} values of (Δ-H_2bie) and (Λ-H_2bie) complexes, tested against the human breast cancer (MDA-MB231) and ovarian cancer (OVCAR-8) cell lines.

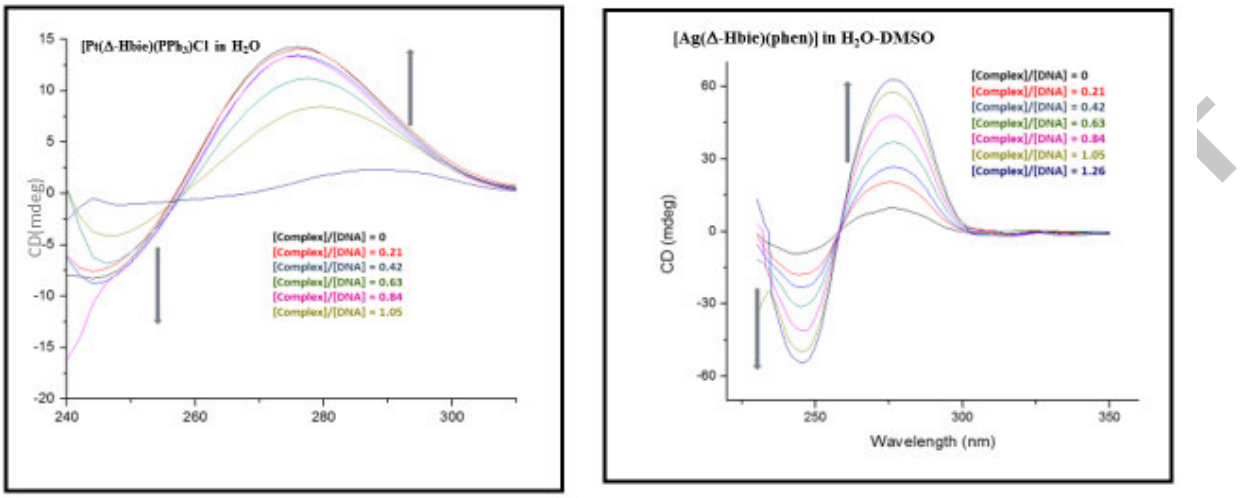

Fig.9: CD spectra of [Pt(Δ-Hbie)(PPh_3)Cl in H_2O and [Ag(Δ-Hbie)(phen)] in H_2O-DMSO

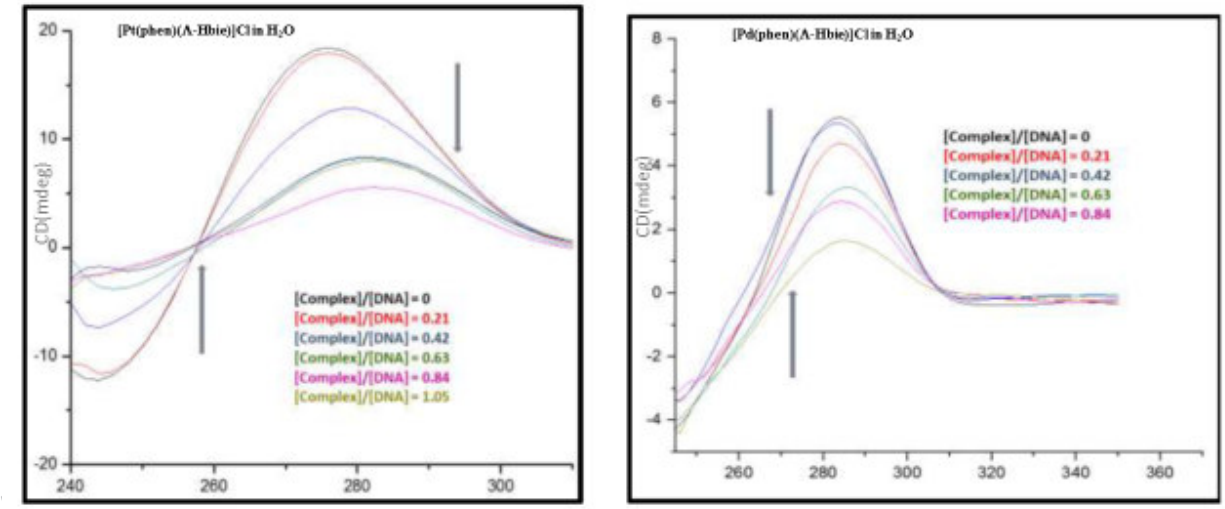

Fig. 10: CD spectra of [Pt(phen)(Λ-Hbie)]Cl and [Pd(phen)(Λ-Hbie)]Cl in H_2O

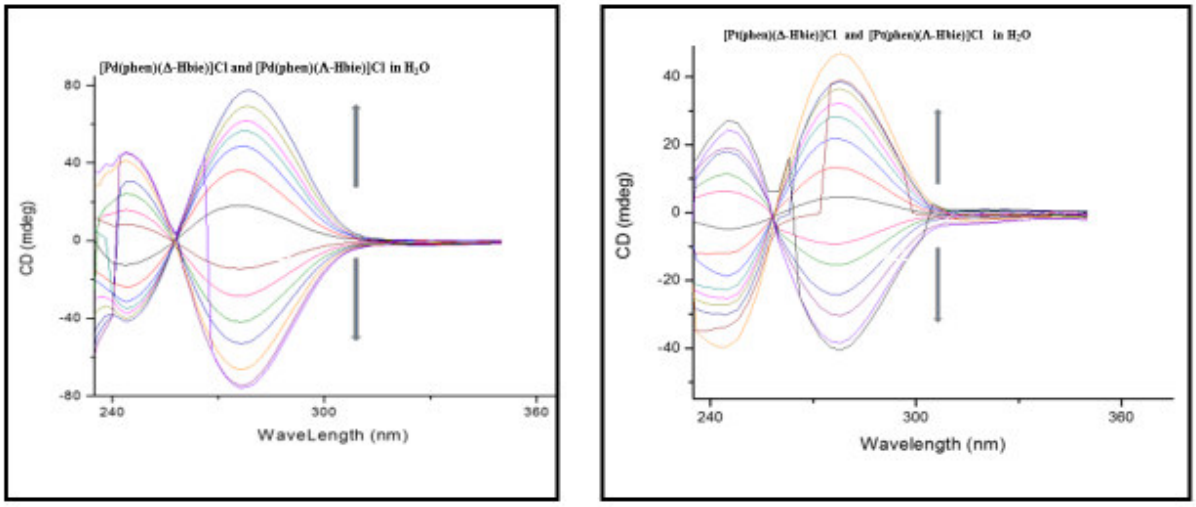

Fig. 11: CD spectra of {[Pd(phen)(Δ-Hbie)]Cl and [Pd(phen)(Λ-Hbie)]Cl} and {[Pt(phen)(Δ-Hbie)]Cl and [Pt(phen)(Λ-Hbie)]Cl} in H_2O

Table 1: ^{1}H-NMR spectral data of Δ-H_2bie and Λ-H_2bie, and their complexes in DMSO-d_6

Compound	H4,H4', H7, H7'	H5,H5', H6,H6'	OH1	OH1'	H_1, H_1'
Δ-H_2bie	**7.49**	**7.12**	**5.99**	**5.99**	**5.25**
Λ-H_2bie	**7.50**	**7.10**	**5.92**	**5.92**	**5.29**
***Cis*-[Pd(Δ-H_2bie)$_2$]Cl_2**	**7.79, 8.04, 8.91[a]**	**7.06, 7.39[a]**	**6.09, 6.15[a]**	**6.21, 631[a]**	**5.89, 5.92[a]**
[Pd(Λ-H_2bie)$_2$]Cl_2	**7.79**	**7.08**	**6.12**	**6.22**	**5.80**
***Cis*-[Pt(Δ-H_2bie)$_2$]$(PF_6)_2$**	**7.50, 7.61[a]**	**7.23, 7.32[a]**	**6.14, 6.21[a]**	**6.26, 6.33[a]**	**5.72, 5.81[a]**
[Pd(Λ-H_2bie)Cl(H_2O)]Cl	**7.62**	**7.15**	**6.17**	**6.30**	**5.82**
[Pt(Λ-H_2bie)Cl(H_2O)]Cl	**7.57**	**7.20**	**6.13**	**--[b]**	**5.65**
[Pd(Δ-Hbie)(bpy)]Cl	**7.8**	**7.30**	**6.04**	**--[b]**	**5.40**
[Pd(Λ-Hbie)(bpy)]Cl	**7.8**	**7.3**	**6.09**	**--[b]**	**5.39**
[Pd(Δ-Hbie)(phen)]Cl	**7.9**	**7.10**	**6.00**	**--[b]**	**5.73**
[Pd(Λ-Hbie)(phen)]Cl	**7.92**	**7.11**	**6.01**	**--[b]**	**5.71**
[Pt(Δ-Hbie)(bpy)]Cl	**7.91**	**7.12**	**6.02**	**--[b]**	**5.58**
[Pt(Λ-Hbie)(bpy)]Cl	**7.94**	**7.09**	**6.01**	**--[b]**	**5.55**
[Pt(Δ-Hbie)(phen)]Cl	**7.95**	**7.13**	**6.03**	**--[b]**	**5.60**
[Pt(Λ-Hbie)(phen)]Cl	**7.99**	**7.16**	**6.04**	**--[b]**	**5.61**
[Ag(Δ-H_2bie)$_2$]ClO_4	**7.65**	**7.20**	**6.10**	**6.24**	**5.63**
[Ag(bpy)(Λ-H_2bie)]ClO_4	**7.99**	**7.41**	**6.14**	**6.34**	**5.61**
[Ag(PPh_3)(Λ-H_2bie)]ClO_4	**7.94**	**7.34**	**6.03**	**6.20**	**5.67**
[Ag(Δ-Hbie)(PPh_3)]	**7.8**	**7.4**	**5.99**	**--[b]**	**5.32**

[a]*cis*-configuration, [b]missed peaks

Table 2: ^{13}C-NMR spectral data of Δ-H_2bie and Λ-H_2bie, and their complexes in DMSO-d_6

Compound	C(1)	C(2)	C(4)	C(5)	C(6)	C(7)	C(8)
Δ-H_2bie	71.60	156.29	134.73	122.18	119.04	121.60	122.20
Λ-H_2bie	71.65	156.32	134.77	122.19	119.09	121.62	122.31
Cis-[Pd(Δ-H_2bie)$_2$]Cl_2	69.77 68.55[a]	154.78 153.71[a]	139.49 139.39[a]	124.81 124.21[a]	118.22 117.00[a]	122.43	132.24
[Pt(Λ-H_2bie)Cl(H_2O)]Cl	70.01	153.99	139.89	124.31	117.99	122.23	131.06
[Pd(Δ-Hbie)(bpy)]Cl	69.22	152.73	139.64	124.56	113.88	123.00	131.40
[Pd(Δ-Hbie)(phen)]Cl	69.18	152.22	140.81	124.51	113.92	123.21	133.39
[Pt(Λ-Hbie)(phen)]Cl	70.00	152.19	140.78	124.50	113.90	123.20	133.38
[Ag(Δ-Hbie)(PPh3)]	69.91	153.60	140.71	125.79	113.41	122.60	132.57

[a]*cis*-configuration

Table 3: Anticancer activity of Δ-H_2bie and its complexes against the human breast cancer (MDA-MB231) and ovarian cancer (OVCAR-8) cell lines

Compounds	IC_{50} μM breast cancer (MDA-MB231) cell line	IC_{50} μM human ovarian cancer (OVCAR-8) cell line
Δ-H_2bie	**>100**	**>100**
[Pd(Δ-H_2bie)$_2$]Cl_2	**93.419 ± 0.3**	**90.330 ± 0.3**
[Pt(Δ-H_2bie)$_2$]$(PF_6)_2$	**94.419 ± 0.2**	**90.803 ± 0.2**
[Pd(bpy)(Δ-Hbie)]Cl	**15.280 ± 0.5**	**15.841 ± 0.3**
[Pd(phen)(Δ-Hbie)]Cl	**2.182 ± 0.3**	**1.477 ± 0.1**
[Pt(bpy)(Δ-Hbie)]Cl	**9.265 ± 0.2**	**9.489 ± 0.4**
[Pt(phen)(Δ-Hbie)]Cl	**1.286 ± 0.1**	**1.552 ± 0.2**
[Pd(Δ-Hbie)(PPh_3)Cl]	**62.020 ± 0.6**	**47.002 ± 0.7**
[Pt(Δ-Hbie)(PPh_3)Cl]	**61.061 ± 0.3**	**45.120 ± 0.3**
[Ag(Δ-H_2bie)$_2$]ClO_4	**24.220 ± 0.4**	**18.080 ± 0.3**
[Ag(phen)(Δ-Hbie)]	**1.403 ± 0.1**	**1.505 ± 0.6**
[Ag(PPh_3)(Δ-Hbie)]	**1.277 ± 0.2**	**1.437 ± 0.2**
Cisplatin	**3.20 ± 0.5**	**2.28 ± 0.6**

Table 4: Anticancer activity of Λ-H_2bie and its complexes against the human breast cancer (MDA-MB231) and ovarian cancer (OVCAR-8) cell lines

Compounds	IC_{50} μM breast cancer (MDA-MB231) cell line	IC_{50} μM human ovarian cancer (OVCAR-8) cell line

Λ-H_2bie	**>100**	**>100**
[Pd(bpy)(Λ-Hbie)]Cl	**52.75 ± 0.4**	**48.204 ± 0.2**
[Pd(phen)(Λ-Hbie)]Cl	**5.781 ± 0.5**	**4.160 ± 0.5**
[Pt(bpy)(Λ-Hbie)]Cl	**35.206 ± 0.3**	**30.422 ± 0.3**
[Pt(phen)(Λ-Hbie)]Cl	**2.846 ± 0.2**	**1.720 ± 0.4**
[Pd(Λ-H_2bie)$_2$]Cl_2	**92.051 ± 0.3**	**93.820 ± 0.3**
[Pd(Λ-Hbie)(PPh_3)Cl]	**67.701 ± 0.5**	**50.221 ± 0.2**
[Pd(Λ-H_2bie)(H_2O)Cl]Cl	**86.770 ± 0.2**	**>100**
[Pt(Λ-H_2bie)(H_2O)Cl]Cl	**98.850 ± 0.2**	**96.980 ± 0.3**
[Ag(Λ-H_2bie)$_2$]ClO_4	**24.590 ± 0.5**	**19.620 ± 0.2**
[Ag(bpy)(Λ-H_2bie)]ClO_4	**5.814 ± 0.6**	**4.161 ± 0.5**
[Ag(PPh_3)(Λ-H_2bie)]ClO_4	**0.443 ± 0.4**	**0.427 ± 0.4**
Cisplatin	**3.20 ± 0.5**	**2.28 ± 0.6**

- Chiral ligands deserve attention as they offer different types of binding site and with a view to enantioselective catalysis, the introduction of chirality in the ligands is an attractive prospect.

- complexes of Pd(II), Pt(II) and Ag(I) based on (Δ)- and (Λ)-1,2–Bis-(1H-benzimidazol-2-yl)-1,2-ethanediol (Δ-H_2bie & Λ-H_2bie) in absence and presence of N,N-chelate and PPh_3 were reported.

- Anticancer activity of the complexes was evaluated against human breast cancer (MDA-MB231) and ovarian cancer (OVCAR-8) cell lines.

- The DNA-binding properties of some complexes were studied using CD spectroscopy.

DNA Interaction and Anticancer Evaluation of New Palladium(II), Platinum(II) and Silver(I) Complexes Based on (Δ)- and (Λ)-1,2–Bis-(1H-benzimidazol-2-yl)-1,2-ethanediol Enantiomers

Ahmed A. Shabana[1], Ian S. Butler[2,*], Annie Castonguay[3], Mohsen Mostafa[1], Bertrand J. Jean-Claude[4], Sahar. I. Mostafa[1,*]

[1] Chemistry Department, Faculty of Science, Mansoura University, Mansoura 35516, Egypt

[2]Department of Chemistry, McGill University, Montreal QC, Canada H3A 2K6

[3] INRS-Institut Armand-Frappier, Institut National de la Recherche Scientifique, Université du Québec, Laval, Canada

[4]McGill University, Royal Victoria Hospital, Department of Medicine, Montreal, QC H3A 1A1, Canada

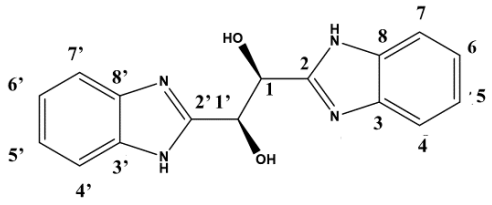

Δ-H_2bie

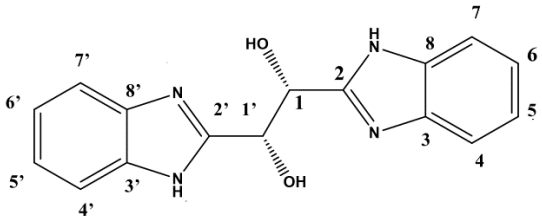

Λ-H_2bie

Structures of (Δ)- and (Λ)-1,2–bis-(1H-benzimidazol-2-yl)-1,2-ethanediol (Δ-H_2bie and Λ-H_2bie)